Live single-cell transcriptional dynamics via RNA labelling during the phosphate response in plants

Sahar Hani, Laura Cuyas, Pascale David, David Secco, James Whelan, Marie-Christine Thibaud, Rémy Merret, Florian Mueller, Nathalie Pochon, Hélène Javot, et al.

RNA labelling in live plants reveals single cell transcriptional dynamics: application to phosphate signaling

#Sahar Hani[1], #Laura Cuyas[1,2], #Pascale David[1], David Secco[3], James Whelan[3], Marie-Christine Thibaud[1], Rémy Merret[4], Florian Mueller[5], Nathalie Pochon[1], Hélène Javot[1], Orestis Faklaris[6], Eric Maréchal[7], Edouard Bertrand[8,9,10*] and Laurent Nussaume[1*]

#These authors equally contributed to the publication

*For correspondance: lnussaume@cea.fr and edouard.bertrand@igh.cnrs.fr

1 Aix Marseille Univ, CEA, CNRS, BIAM, UMR7265, SAVE (Signalisation pour l'Adaptation des Végétaux à leur Environnement), Saint-Paul lez Durance, France.

2 Centre Mondial de l'Innovation, Groupe Roullier, 18 avenue Franklin Roosevelt, Saint-Malo, France.

3 Department of Animal, Plant and Soil Sciences, Australian Research Council Centre of Excellence in Plant Energy Biology, School of Life Sciences, La Trobe University, Bundoora, Victoria, Australia.

4 UMR5096 CNRS/Université de Perpignan, Laboratoire Génome et Développement des Plantes, 58 Avenue Paul Alduy, Perpignan, France

5 Unité Imagerie et Modélisation, Institut Pasteur and CNRS UMR 3691, 28 rue du Docteur Roux, 75015 Paris; France

6 MRI, BioCampus Montpellier, CRBM, Univ. Montpellier, CNRS, Montpellier, France.

7 UMR 5168 CNRS-CEA-INRA-Université Grenoble Alpes, Laboratoire de Physiologie Cellulaire et Végétale, iRIG, CEA-Grenoble, 17 rue des Martyrs, Grenoble, France.

8 Institut de Génétique Moléculaire de Montpellier, Univ. Montpellier, CNRS, Montpellier, France.

9 Institut de Génétique Humaine, Univ. Montpellier, CNRS, Montpellier, France.

10 Equipe labélisée Ligue Nationale Contre le Cancer, Montpellier, France.

Abstract

Plants are sessile organisms constantly adapting to ambient fluctuations through spatial and temporal transcriptional responses. Here, we implemented the latest generation RNA imaging system and combined it with microfluidics to visualize transcriptional regulation in living Arabidopsis plants. This enabled quantitative measurements of the transcriptional activity of single loci in single cells, real time and changing environmental conditions. Using phosphate responsive genes as model, we found that active genes displayed high transcription initiation rates (~3s) and frequently clustered together in endoreplicated cells. We observed gene bursting and large allelic differences in single cells, revealing that at steady-state, intrinsic noise dominated extrinsic variations. Moreover, we established that transcriptional repression triggered in roots by phosphate, a crucial macronutrient limiting plant development, occurred with unexpected fast kinetics (~minutes) and striking heterogeneity between neighboring cells. Access to single cell RNA polymerase II dynamics within live plants will benefit future studies of signaling processes.

Introduction

Plants are sessile organisms permanently coping with environmental variations. Transcriptional reprogramming[1] plays a key role in these responses as illustrated by the number of plant transcription factors (5.4% in Arabidopsis, https://agris-knowledgebase.org/). Most physiological studies quantify mRNA abundance in organs. Accessing specific cell types is possible by expressing a fluorescent marker in cells of interest, to FACS sort them and perform sequencing analysis[2]. Nevertheless, this requires long enzymatic digestion to generate protoplasts preventing fast kinetic studies. Transcriptional fusions between promoters and reporter genes such as GFP provide cellular resolution, but the time required to accumulate detectable level of mature fluorophore (often in the range of tens of minutes[3]) prevents the rapid transcriptional monitoring. This is moreover highly variable and depends on the strength of the promoter studied and the microscopy setup, leading to confounding effects. These considerations are even more crucial when studying transcriptional inhibition. The above-mentioned experiments provide access to total RNA (or protein), resulting from the balance between synthesis and degradation. Many fluorescent proteins decay in the range of hours and RNA degradation is highly variable from one gene to another[4,5]. For instance, the median half-life value of *Arabidopsis* mRNAs is 107 min, but exceeds one day for many messengers[4]. This is far too long for transcriptional responses occurring within seconds such as for instance during light stress [6].

All these issues can be resolved with a method originally developed for yeast and animal granting direct real time access to transcriptional activity at the level of single cells[7-10]. It is based on a fusion between GFP and the bacteriophage MS2 coat protein (MCP-GFP)[7,8] or on related systems[11]. The MCP-GFP recognizes a specific RNA stem-loop inserted in multiple copies into a reporter RNA, promoting MCP-GFP multimerization to provide signal bright enough for single RNA visualization[9]. Importantly, binding occurs during RNA synthesis and

monitors transcription in real time. In plants, this technology would offer major advantages for physiological studies such as adaptations to biotic and abiotic stresses. Indeed, it grants access to the variability of all cell types providing ways to understand how the activity of single cells is integrated within tissues or organs and thus to better understand gene regulation. Real time quantitative analysis can be performed for transcription initiation, elongation or gene bursting. This last phenomenon can further be used to identify promoter states that are rate-limiting for transcription initiation, and thus likely points of regulation[12]. The MS2 technology also allows the identification of extrinsic and intrinsic sources of transcriptional noise

Therefore, we implemented it into plants using state-of the art MS2x128 repeats to tag a single RNA with ~250 to 500 GFPs for optimal detection sensitivity[13]. We used this system to analyze the transcriptional response to a major macronutrient: inorganic phosphate (Pi). Pi deficiency triggers major transcriptional modifications affecting plant development and metabolism [14,15]. These are mainly controlled by master regulator genes of the PHR1 family[15-17]. Being constitutive, their regulatory activity relies on inhibitors of the SPX family tuned by Pi uptake[18,19] as they inhibit PHR1 activity only in the presence of Pi metabolites [20,21].

Here we used the promoter of early Pi responding genes to drive transcription of an MS2x128 reporter. We combined fast quantitative imaging and microfluidics[22], to precisely control Pi delivery while providing stable environmental conditions. It revealed a high heterogeneity of responses between adjacent cells and identified the rapid perception of Pi by the root (within 3/5 min) validating the power of the MS2 technology to dissect plant transcriptional regulation.

Results

Phosphate resupply promotes rapid transcriptional modifications

To identify early markers sensitive to phosphate, we starved plants and performed Pi refeeding experiments. After addition of Pi in the liquid culture medium, we harvested roots and leaves after 30, 60 and 180 min for RNA-seq analysis. In roots, only 22 genes exhibited a significant two-fold reduction of their transcript level over the three time points (Fig. S1A-B). Analysis of the shoot samples revealed a delayed reduction of all these markers in aerial parts (only one third were repressed after 30 min) indicating that Pi was first perceived by roots. Independent experiments analyzed by RTqPCR using well known markers for Pi starvation[15,23], involved in Pi uptake (*PHT1;4*) or Pi-induced metabolic remodelling (*SQD2*), confirmed these results (Fig. 1A and S1B). The rapid down-regulation observed also highlighted the fast turn over of these transcripts (half-life estimated to 15-30 minutes; Fig. S1A-B), in regard to the Arabidopsis median value of 3.8 hours[5]. For the rest of this study we selected two genes (*SPX1* and At5G20790, named hereafter *UNI1* for Unicorn1), which combined the highest levels of expression in Pi depleted medium (-Pi) with broad dynamics as measured by +Pi/-Pi fold change.

Regulation was assumed to occur mainly transcriptionally, as the transcriptional inhibitor cordycepin mimicked effect of Pi resupply (Fig. 1A). This was confirmed by transcriptional fusions with luciferase, which conferred to the reporter gene a similar temporal response to Pi resupply (Fig. S1C), whereas fusing a CaMV 35S constitutive promoter to the coding region of the markers did not reveal any significant difference of RNA levels between +Pi (after 180 min refeeding) or -Pi conditions (Fig. S1D), except for short transient induction promoted by the stress of Pi addition observed during first hour following resupply. A sequence analysis of the 22 genes identified above revealed the presence of P1BS regulatory

boxes[16] in 95% of the cases. This box is the binding site of master regulators belonging to PHR1/PHL1 family. Addition of Pi promotes synthesis of inositol pyrophosphates, which act as a molecular tether to fix members of the SPX family to PHR1 and inhibit its activity[20,21] (Fig. 1B). Consistently, the induction of *SPX1* and *UNI1* during Pi starvation was nearly fully abolished in *phr1/phl1* double mutants, which suppress a majority of PHR1/PHL proteins (Fig. 1C). Moreover, this was observed for 91% of the 22 genes identified (Fig. S1A[17]). SPX family members inhibit PHR1 and the analysis of *spx1/spx2* double mutants further revealed that reducing the SPX protein pool delayed the repression triggered by Pi addition (Fig. 1D). Altogether, these results demonstrated that the fast decrease of the 22 transcripts identified here resulted from transcriptional control involving several key players such as PHR or SPX family of proteins. Of note, classical transcriptional fusion with Luciferase did not report a fast transcriptional repression (Fig. 1E). More than one hour was required to observe a significant decrease of the signal, whereas RTqPCR failed to detect a significant reduction of mRNA levels for at least 15-20 minutes after resupply (data not shown). To better characterize the transcriptional response to Pi resupply, we implemented the MS2 system for RNA labeling, a technology so far restricted mostly to animal and yeast but offering unique spatio-temporal resolution to study transcriptional regulation.

Generation and validation of MS2-tagged Arabidopsis lines

We used the last generation MS2 tag containing 128xMS2 repeats, originally developped to image single-molecule of HIV-1 RNA[13]. To improve RNA folding and prevent plasmid instability, this construct is made of 32 distinct MS2 stem loops replicated four times, with each stem-loop binding dimers of the MCP protein with sub-nanomolar affinity[13] (Fig. 2A). In animal cells, this extended tag provides about a five-fold improved sensitivity over the original MS2x24 tag and allows single molecule visualization for extended periods of times

143 even at high frame rates[13]. Moreover, this construct bears the lower affinity variant of the
144 MS2 stem-loops (U instead of C in third position of the loop), providing excellent RNA
145 visualization while preserving normal RNA degradation[24].

146 We developped Moclo vectors adapted to the Golden Gate system[25] to facilitate the
147 cloning and use of the MS2x128 recombinogenic sequence (Fig S2A), and we generated
148 transcriptional fusions with the *SPX1* and *UNI1* promoters (Fig. 2A). We then introduced into
149 the binary vector used for plant transformation a gene expressing a nuclear targeted MCP-
150 eGFP fusion protein[13] under the control of the weak constitutive Ubiquitin-10 promoter[26] (Fig
151 S2A). For the two constructs, genetic analysis selected homozygous transformants exhibiting
152 single locus insertions. We first focused on the homozygous pSPX1::MS2x128 line named 'S'
153 for strong and exhibiting the best signals. Molecular analysis revealed the insertion of three
154 copies of the transgene at a single locus in the S line (Fig S3). The presence of the cap and the
155 polyA tail, crucial elements for RNA stability, was also verified for MS2x128 transcripts (Fig
156 S4). Single-molecule fluorescence in situ hybridization (smFISH) was performed on root
157 squashing to analyze the phosphate response of the transgenes. Root squashes allows good
158 probe penetration in tissues and causes some cells to fall off the root and adhere to coverslips
159 as a monolayer[27], allowing high quality imaging using wide-field microscopy with high
160 numerical aperture objectives (Fig. 2B and S2B). The fluorescent oligonucleotide probes
161 hybridizing against the MS2 stem-loops labelled the reporter RNA in most tissues of the root
162 grown on Pi depleted medium, including the root cap and mature tissues (Fig. 2B and see
163 below Fig. 3), and they did not detect signals in Col0 negative controls lacking the transgene
164 (Fig. S5). Interestingly, the smFISH signals were rarely detected in the cytosol and mostly
165 stained nuclei where transcription sites were visible as bright spots. This nuclear localization
166 could be due to either a nuclear retention of the MS2-labelled RNA, or a reduced stability in
167 the cytosol. In any case, the smFISH signal disappeared when plants were grown in the

presence of phosphate (Fig. 2B, right panels). Quantification of the signals indicated that 74% of the cells expressed the pSPX1::MS2x128 transgene in absence of phosphate (>20 RNA/cell), and none in its presence (Fig. 2B and 2D). To further validate these results, we visualized the endogenous *SPX1* transcripts with a mix of 24 fluorescent oligonucleotide probes specific for SPX1. In Pi depleted conditions, the probes identified the transcription sites and single mRNA molecules present in the cytoplasm, as expected for a translated transcript (Fig 2C and S2B). Similar to the pSPX1::MS2x128 reporter, the endogenous *SPX1* mRNA was expressed throughout the root, including the cap and mature tissues[28], with a number of positive cells similar to that of the reporter (Fig. 2D). Importantly, *SPX1* smFISH signals were very low in plants growing on Pi rich medium (Fig 2D and 2C, right panels) and completely absent in a *spx1spx2* double mutant used as negative control (Fig S6). Overall, these data indicated that the MS2 transgene driven by the *SPX1* promoter faithfully reported on the expression of *SPX1*, with a similar regulation and spatial expression pattern.

Imaging transcription in fixed tissues of whole plants with MCP-GFP

We then turned to spinning disk confocal microscopy to image plants through the tissue depth (reaching 100µm) and to assess in detail the performance of MCP-GFP to image transcription. We first used the brightest homozygous pSPX1::MS2x128 line (called S) to image expression of the reporter in the root (Fig. 3A; a viewer with a zoomable high resolution image can be accessed at https://imjoy.io/lite?plugin=muellerflorian/hani-ms2:hani-ms2-sample-3 and https://imjoy.io/lite?plugin=muellerflorian/hani-ms2:hani-ms2-sample-1, which is a continuously growing organ with a well-defined architecture. At the apex, the root cap encapsulates the meristematic zone where cells divide rapidly until they enter the transition zone (TZ). Cells then elongate (EZ) and initiate tissue differentiation

192 according to a well defined radial pattern, generating a number of different cell types (Fig.
193 3A).

194 First, we tested whether MCP-GFP could faithfully report on the MS2-tagged RNA
195 and we performed smFISH together with MCP-GFP imaging. In the root cap, which is mostly
196 composed of diploid cells[29], smFISH against the MS2 stemloops revealed both single
197 molecule and transcription sites, visible as bright spots in the nucleus (Fig. 3B, bottom panels;
198 pink and orange arrows, respectively). In both root cap (Fig. 3B) and mature tissue (Fig. 3C),
199 we observed colocalization between the smFISH signals revealed by MS2 probes and the
200 fluorescent signal produced by MCP-GFP. The transcription sites were easily detected (Fig.
201 3B and C, orange arrows), and MCP-GFP could also reveal the brightest single mRNAs (Fig.
202 3B, pink arrows), indicating that the sensitivity of the system approches that of single
203 molecules (see also below live cell experiments). To assess the reliability of detection, we
204 counted transcription sites in both colors, and found that 90-95% of the sites detected by
205 MCP-GFP were also labelled by MS2 smFISH.

206 Finally, we extended these observations to other *Arabidopsis* lines, using plants having
207 either the pUnicorn1::MS2x128 reporter or another single locus transformant of the
208 pSPX1::MS2x128 transgene (J line). The J line turned out to also present multiple T-DNA
209 copies (Fig S3B), but it exhibited reduced levels of fluorescence when compared to the S line.
210 The transcription sites of the reporters were readily detected with MCP-GFP and co-localized
211 with the MS2 smFISH signals (Fig. S7). Overall, these results validated the MS2/MCP
212 system as a robust and sensitive system to image transcription in whole plants tissues.

213

214 **Single molecule counting by smFISH gives insights into the dynamics of transcription in**
215 **Arabidopsis *thaliana***

The ability of smFISH to detect single RNAs enables a quantitative analysis of the RNA polymerase II transcription cycle[9,12,30,31]. We therefore measured the brightness of transcription sites and used the visible single molecules to compute the absolute number of nascent RNA molecules at active transcription sites (Fig. 4A and B; see Methods). We obtained an average of 37 molecules at the transcription site of the pSPX1::MS2x128 reporter for the S lines, with a main peak at ~20 molecules (Fig. 4A). We also designed a set of 21 fluorescent oligonucleotides against the sequence immediately downstream the polyadenylation site of the reporter (see Fig. S12). We however failed to detect any smFISH signal, indicating that 3'-end processing was rapid as compared to transcription. This agrees with previous GRO-seq experiments that revealed that RNA polymerases terminate transcription very rapidly after polyA sites[32,33]. We repeated these measurements for the endogenous *SPX1* mRNA and found an average of 11.3 molecules at transcription sites, with a main peak at 9 molecules. Given that the *SPX1* gene is 1.4 kb long, this number suggests that active *SPX1* genes have one polymerase every 77 bases if 3'-end processing is immediate, and one polymerase every 120 bases if 3'-end processing takes a minute[13] (assuming an elongation rate of 2 kb/min[30]). For the 3kb pSPX1::MS2x128 reporter, similar numbers were found if one considers that the peak of 25 molecules at a transcription site corresponds to a single active copy (Fig. 4A). These numbers indicate that active *SPX1* genes have an initiation event every 2.3 to 3.5 seconds on average (see Methods and schematic in Fig. 4B). This is in the high range of previous estimates obtained in human cells and Drosophila[13]. It suggests that transcription in *Arabidopsis* is rapid and occurs in the form of polymerase convoys, produced by initiation events rapidly occurring one after another when the gene turns on[13].

Quantitation of *SPX1* transcription in fixed roots reveals cell polyploidy in mature tissue as well as large allelic differences

241 Endoreplication occurs frequently in root with DNA cell contents ranging from 2C to 16C[29].
242 This phenomenon increased as one moves away from the root tip. Being involved in the size
243 of the cells, it also varies and increases from the central to the expended external cell layers
244 such as cortex or epidermis[29] (Fig. 3A). The number of transcription sites present in each
245 nucleus highlighted this endoreplication. In the root apex of the pSPX1::MS2x128 S line,
246 cells of the columella (extremity of the root cap) exhibited in the vast majority of cases no
247 more than two transcription sites for the MS2 reporter or the endogenous *SPX1* gene, as
248 expected for a mainly diploid tissue[29] (Fig. 3B and Fig. 4C for quantifications). In contrast,
249 images recorded in the differenciated part of the root revealed the more complex nature of
250 older tissues with the presence of cells with many transcription sites, indicating polyploidy
251 (Fig. 3C and 2C). Quantification of the number of active alleles per cell indicated that in
252 diploid columella cells, only 3% of the cells had more than 2 transcription sites, while in the
253 mature tissue, 35% had more than two sites, with 2% having as many as 7 (Fig. 4C and 4D).
254 Similar numbers were obtained with the endogenous *SPX1* gene (Fig. 4D). Interestingly, we
255 noted that in cells with many active alleles, the *SPX1* transcription sites frequently clustered
256 in the nucleoplasm, most often forming two groups (see Fig. 4F for an example). To explore
257 this further, we measured the distance between all visible transcription sites in cells having 4
258 to 8 active sites, and we compared the resulting distance distribution to a situation were we
259 simulated 8 sites with a random location (Fig. 4E, see Methods). This showed that the
260 transcription sites had a non-random distribution and were frequently close to one another,
261 with 40% of the distances falling within 1.5 microns. This phenomenon was also visible when
262 we compared the brightness of transcription sites in cells having one or two transcription
263 sites, to cells having four or more sites (Fig. S2C). Cells with one or two SPX1 transcription
264 sites had a single peak of 10 nascent RNAs, while cells with four or more sites had a second
265 peak at 20 nascent RNAs (Fig. S2C). This suggests that in these cells, some transcription sites

266 had coalesced into a single spot, reminiscent of the 'transcription factories' previously
267 described in human cells[34].

268 Next, we compared the activities of the different alleles of single cells, focusing first
269 diploid root cap cells. Surprisingly, an important number of cells exhibited only a single
270 active transcription site (30 % of the cells; Fig. 4C), or no transcription at all (39%). This was
271 also observed with the endogenous *SPX1* gene (Fig. 4D), indicating that it is a feature of this
272 Arabidopsis gene and not an artifact of the MS2 reporter. Since the cells with no transcription
273 sites contained smFISH signal in the nucleoplasm or the cytoplasm (Fig. 3), transcription had
274 been active in these cells, therefore indicating that *SPX1* promoter activity was discontinuous.
275 Such discontinuous transcription is the result of gene bursting and has been oberved in many
276 organisms including yeast, Drosophila and mammals[35]. To our knowledge, it has not been
277 reported so far in plants. Gene bursting involves the stochastic switching of a promoter
278 between active and inactive states. It depends on mechanistic aspects of transcription
279 initiation as well as transcriptional regulation[12]. This stochasticity causes variations in gene
280 expression among identical cells (ie. gene expression noise), which has sometimes important
281 phenotypic consequences[12]. Commonly, two sources of noise are distinguished: intrinsic and
282 extrinsic. Intrinsic noise is due to the stochastic nature of biochemical reactions involving a
283 single molecule of DNA and the transcription factors acting on it, and it occurs independently
284 on each allele. In contrast, extrinsic noise modulates similarly both alleles as the result of
285 events affecting the entire cell (such as cell cycle or activation of a signaling pathway).
286 Interestingly, our capability of accessing several alleles within a cell raised the possibility to
287 discriminate between the two causes of transcriptional noise. For each cell that had only one
288 or two active alleles, we plotted the brightness of one *SPX1* allele as a function of the other
289 (Fig. 4G). This revealed both correlated (cells on the diagonal) and uncorrelated (cells off the
290 diagonal) transcriptional activities of these alleles. To quantify this phenomenon further, we

measured the total, intrinsic and extrinsic noise[36,37], using cells having either exactly two, or 3-4 active transcription sites (Fig. 4H, see Methods). As expected from the results described above, we found that the total noise had significant intrinsic and extrinsic contributions, with intrinsic noise being the dominant source. This highlights the quantitative importance of transcriptional noise for Arabidopsis.

Real-time visualization of SPX1 transcription reveals gene bursting and Pi mediated repression

We used a simplified version[38] of the RootChip microfluidic system[22] to combine live-cell imaging with the capacity to change the phosphate solution rapidly (Fig. 5A and Movies). Imaging was performed with spinning disk microscopy, which offered the best compromise between image quality, size of the field of view and image acquisition speed. A typical experiment recorded at each time point a z-stack of 200 images with a z-spacing of 500 nm, allowing us to image at high resolution the entire root and thus access all its tissues. One image stack was recorded every 2-3 minutes for ~1 hour, and maximum intensity projection produced clear images where multiple transcription sites could be analyzed. Using the brightest S line expressing pSPX1::MS2x128 and grown without Pi, images from the first time point confirmed the transcriptional heterogeneity between cells, with neighboring cells exhibiting zero, one, two or even more active transcription sites and with the intensity of transcription sites varying by a factor of 4 (Fig. 5-7 and Movies 3-7). Observation of the root constantly supplied with -Pi solution directly demonstrated bursting of the SPX1 promoter, with transcription sites coming on and off over periods of minutes (Fig. 6, Movies 1 and 2). Interestingly, this phenomenon was mainly observed in the root cap, and only very rarely in mature tissues. Remarkably, the arrest of transcription after a burst provided an opportunity to visualize the release of single RNAs from the transcription sites (Fig. 6D, Movie 2),

316 highlighting the dynamics of the process and confirming single molecule sensitivity in live
317 plants.

318 Next, we analyzed the response to Pi resupply. To this end, the S line was first grown
319 during a few days in -Pi liquid medium, before receiving phosphate rich medium combined
320 with the Synaptored^{TM} fluorescent dye. This allowed to precisely record the arrival of the
321 supplemented media on the imaging field, thereby defining the time 0 of the time course. The
322 movement of nuclei in the cells and the displacement of cells themselves complicated
323 transcription site tracking. To simplify the analysis of the time course, we therefore used only
324 cells with one or two active transcription sites. The repression of transcription upon Pi
325 resupply proved to be rapid (Fig. 5 A-C, S8, S9 and Movies 3-7). Signals were then
326 normalized to the value obtained at time 0 (Fig. 7C) and an average response curve was
327 produced (Fig. 7D). The measurements were repeated with independent samples and they all
328 showed similar curves with a signal starting to decrease between 0 to 6 minutes after Pi
329 provision at the root surface (Fig. 7E). Similar results were obtained with independent
330 transgenic J line (Fig. S10, Movie 8), revealing the extraordinary sensitivity and rapidity of
331 the regulatory cascade triggered by Pi.

332 The decrease of fluorescence starting with Pi resupply reached the root continued until
333 it reached a plateau 18 to 25 minutes later (Fig. 7F and S10). Interestingly, cells presenting
334 multiple transcription sites revealed on average a close coordination of the repression between
335 these sites, indicating that extrinsic factors dominate gene regulation when Pi repression
336 initiates, as expected for a signaling pathway affecting the entire cell (Fig. 5C, 7B and S8).
337 Controls continuously supplied with Pi depleted solution in mature tissue did not show
338 significant changes (Fig. 7 G, H and S11) over 25 min observation period.

339 The comparison between the MS2 and RTqPCR results revealed a delay of 20-30
340 minutes for the RT-qPCR to show the maximum repression, which is in agreement with the

SPX1 mRNA half-life previously estimated in the range of 15-20 min (Fig. 1A and S1A,B). Overall, these results demonstrate the unexpectedly fast dynamics of the plant response to Pi resupply, and nicely illustrates the capacity of the MS2 system to access transcriptional regulation in live plants. It should be noticed that in mature tissues, we restricted the analysis to nuclei exhibiting one or two active alleles to avoid misattribution during the analysis (resulting from nuclei movement during analysis). This favors more central cell (less affected by polyploidy) representation, which are known to be less affected by Pi repression compared to cortex or epidermis cells[39]. This may explain the slight difference (around 10%) of average extent of the decrease in expression between RTqPCR and MS2 live imaging.

Discussion

Large MS2 arrays and microfluidics reveal single cell transcriptional dynamics in live plants

Fluorescent RNA technologies provide access to single molecule studies offering invaluable insights into gene expression mechanisms[12,40]. A previous attempt to use these technologies in plants studied a highly abundant viral RNA in transient transformants and low signal-to-noise ratio prevented their use in stable plant lines[41]. The MS2x128 construct developed here (which uses six time more MS2 loops) solves this problem and provides a direct acces to transcriptional activities of live plants, at the level of single alleles and with a sensitivity nearing single RNAs. Nevertheless, single molecule detection remains difficult and not exhaustive, due in particular to the necessity of limiting illumination power to prevent bleaching and phototoxicity when acquiring 200 z planes for tens of time points. We hope that new constructions currently underway, where the number of MS2 loops is doubled (256) or MCP-GFP expression is optimized, will provide important future improvements. Originally developped for yeast or mammalian cell lines, fluorescent tagging of RNA has been introduced in only few multicellular organisms (Drosophila embryos in particular[10,35]), mostly

to study transcriptional regulation during embryonic development and in absence of external perturbations. Here, the implementation of microfluidics allowed a complete control of environmental conditions and the investigation of the root response to phosphate starvation and resupply. Measurements of transcriptional inhibition often suffer from both indirect measurements introducing a considerable lag time in repression detection, and ensemble measurments averaging effects. In contrast, the tools developed here allow visualization of repression in real time and single cells, and demonstrate that it is a very rapid process that takes place in minutes.

Plants are sessile organisms that developed exquisitely efficient regulation systems to ensure homeostasis in face of changing environmental conditions. Due to the fast and sensitive tuning of transcriptional mechanisms, microfluidics offers the ideal solution to control environmental conditions. This strategy could be extended to a variety of other stresses, including biotic ones, and to all plant organs as various microfluidic systems exist to study aerial parts. The technological developments made here thus open entirely new possibilities by allowing the direct visualization of transcriptional regulations in living plants, in real time and at the level of single cells and single molecules.

Integration of single cell responses to phosphate signaling at the tissular level

The capacity to dissect transcriptional responses of individual cells within a tissue and between different tissues within an organ is a major step forward. The use of real-time phosphate radioisotope imaging revealed that Pi enters and accumulates in the root tip within less than one minute [42]. The present study thus directly links this arrival with transcriptional repression, demonstrating the close concomitance between the two phenomena. Moreover, our analysis, owing to unprecedented cellular resolution in plants, also identified the heterogeneity of transcriptional responses. Indeed, we observe strikingly different responses

393 to phosphate resupply in different tissues of the root: a cell can repress *SPX1* transcription
394 within minutes while its neighbor may continue transcribing unabatedly (Fig. 3B, 5C and 7).
395 The fact that the alleles of a cell show a coordinated response indicates that this heterogeneity
396 in repression arises mainly from extrinsic sources, as expected for a regulation involving a
397 cellular signaling pathway. Interestingly, the cell-to-cell heterogeneity of *SPX1* transcription
398 is already visible at steady state when plants are starved from phosphate: a third of root cap
399 cells contain *SPX1* mRNAs while not being transcriptionally active, indicating discontinuous
400 promoter activity. This peculiar phenomenon of gene bursting is an important driver of cell
401 heterogeneity and has already been described in animals[35], but not plants. Our analysis
402 suggested that this phenomenon may differ greatly between cell types. Using specific cell
403 layer markers in the future will help to investigate more precisely this phenomenon and
404 decipher putative driving mechanisms. We show here with *SPX1* that transcriptional noise in
405 plants has both intrinsic and extrinsic components, suggesting that it arises from both
406 stochastic promoter dynamics and cellular regulatory pathways. At steady state, in absence of
407 Pi, intrinsic noise appears to be dominant, while extrinsic factors appear to take over during Pi
408 refeeding, generating heterogeneity in repression kinetics and in the extent of repression. This
409 needs to be investigated in different organs, developmental stages, physiological statuses and
410 environmental contexts. Because of its role in cell heterogeneity, transcriptional noise is
411 clearly a key point to understand how the activity of individual cells is integrated within entire
412 tissues.
413
414 **Transcription imaging in polyploid cells reveals clustering of active alleles**
415 Endoreplication in plants has been associated with high metabolic activity or fast biomass
416 development, economically important for most vegetables and fruits. Recent analysis of
417 Arabidopsis illustrated the extent of this process affecting many root cells during their

development and differentiation, the highest level of endoploidy (16C) being observed either in most developped cells (epidermis hair cell) or in highly active regions associated with distribution of nutrients (phloem companion cells)[29]. So far endoploidy detection uses destructive techniques such as flow cytometry or histochemical staining of endocycles markers or DNA. Here, we overcame such limitations providing the opportunities to access kinetics of endoploidy taking into account development, cell fate, biotic or abiotic stresses. Our results highlighted the magnitude of somatic polyploidy in a root, revealing that many alleles of polyploid cells can be simultaneously transcriptionally active. We found that in absence of phosphate, active *SPX1* alleles of polyploid cells tended to cluster together, possibly because endoreplicated chromatids generally occupy the same chromosome territory[43]. More surprisingly,our data also suggest that active SPX1 alleles have a propensy to coalesce together, a phenomenon reminiscent of transcriptional factories reported in animal cells[34]. In the future, it will be important to confirm the coalescence of active alleles by directly observing this phenomenon in live cell. It will be also interesting to determine whether this is related to the very high transcriptional activity of the *SPX1* gene in these conditions (one initiation event every 2-4 seconds), and to understand how this process occurs and whether it contributes to gene regulation. Note that these initiation rates are based on polymerase elongation speed measured in animals or yeast. They do not take into account possible modifications affecting transcription elongation, pausing and termination, which are poorly described in plants despite recent advances[32,33], and will require additional experiments to account for them.

Overall, the technology presented here offers direct access to the RNA polymerase II activity in live cells and could be used to study crucial plant phenomena affecting transcription (silencing, heterozygosity, impact of gametophyte origin …). This unprecedented spatio-

443 temporal resolution for plant transcription therefore provides new horizons to multiple
444 applications hitherto inaccessible for plant physiology.

Material and Methods

Plant materials and growth conditions

Wild type Arabidopsis thaliana Col-0 seeds were sterilized and grown vertically on Murashige and Skoog medium diluted 10-fold (MS/10) in Petri dishes supplemented with a Pi source containing either 500 µM (+P) or 13 µM (-P) KH_2PO4 in a culture chamber under a 16-hr- light/8-hr-dark regime (25°C/22°C), as previously described[44].

For global transcriptomic analysis, 7 days old seedlings were germinated on a sterile nylon mesh deposited at the surface of the culture medium to facilitate the transfer between media. For resupply experiment, plantlets were transferred from -P to +P for 30, 60 or 180 minutes. In order to minimize stress related transfer, control plants in -P and +P media were also transferred for similar period of time on same media.

In order to get closer to microfluidic conditions and limit the stresses related to the solid media transfer, we modified the protocol for subsequent experiments (RTqPCR analyses), by transferring the 7 days old seedling from agar plate to liquid MS/10 for 3 days. Then, -P plants were resupplied with +P solution for up to 3 hours before collecting the roots for RNA extraction. Transcription inhibition experiments were performed by addition of 0.6 mM cordycepin [45]. For each condition three independent biological replicates were analyzed. Plant DNA extraction and genetic segregation analysis were performed as previously described[46].

RNA-seq library preparation and analysis (RNA seq and RTqPCR)

The extraction of total RNA from Arabidopsis roots or shoots, the synthesis of RNA-seq libraries and their analysis using Illumina sequencing technology (Illumina, San Diego, CA) were performed as previously described [47]. Quantitative RTqPCR experiments were performed as previously described [48] with primers listed in the Supplemental Table 1.

For 7-Methylgunaosine RNA Immunoprecipitation (m7G-RIP) experiment, total RNA was extracted using Monarch Total RNA Miniprep kit including DNAse treatment on column (New England Biolabs). m7G-RIP was then performed as previously described[49] with slight modifications. 5 µg of total RNA was used as starting material. Elution was performed using Guanidium 8M 10 minutes at 65°C followed by RNA precipitation. As negative control, pyrophosphatase treatment was performed on total RNA prior to m7G-RIP. Reverse-transcription was then performed on input and eluate fractions using 500 ng of RNA and oligo dT primer. PCR was then performed using primers against MS2 transgene or endogenous SPX1 using oligos described in Supplemental Table 1.

Transgene constructs

The pSPX1::MS2x128 and pUNI1::MS2x128 constructs were built using the Golden gate cloning technique [25]. MS2x128 stem loops (pMK123-MS2X128-XbaI) and NOS terminator were inserted into level 0 vectors pICH41308, and pICH41421 respectively. The promoters of *SPX1* (At5G20150) and *UNICORN1* (At5g20790) were PCR amplified (1452 bp[28] and 2161bp upstream of the start codon) using oligos described in Supplemental Table 1. These sequences were introduced in level0 vectors (pICH41295). The levels 0 modules were assembled directly into a level2 expression vector pICH86966.

The Ubiquitin10 promoter (At4g05320) driving eGFP expression derived from pUBN-Dest[26] was assembled with MCP contained in pDONR201[8] using the Gateway cloning technique (Invitrogen) creating plasmid pUb::eGFP/MCP-NLS. This construct was excised from the Gateway vector using PmeI and SmaI (Invitrogen) and introduced in level2 T-DNA pSPX1::MS2x128 or pUNI1::MS2x128 vectors using PmeI restriction sites. A clone having the two constructs in opposite orientations creating pMCP/proSPX1::MS2 was used to transform Agrobacterium tumefaciens strain C58C1. Figure S2A summarizes the cloning

strategy. The reporter line carrying Luciferase in fusion with the UNICORN1 promoter was generated as previously published [44].

Production of transgenic lines

Transformants produced by floral dipping[50] were selected on Hoagland/2 media complemented with 50 mg/L kanamycin. The progeny exhibiting 3:1 segregation were carried to T3 generation to identify homozygous lines carrying a single insertion locus. At least 5 independent lines were obtained for each construct.

Single molecule Fluorescence *In Situ* Hybridization

Arabidopsis seedlings were grown on +P and -P agar media. The roots of 7 to 10 day old seedlings were collected and fixed for 30 min with 2-(*N*-morpholino) ethane sulfonic acid (MES) buffer solution pH 5.7 containing 4% paraformaldehyde (32% methanol-free solution; Electron microscopy Sciences). pH was adjusted to 5.7 with KOH solution.

Roots were rinsed twice with MES buffer (pH 5.8) and put onto a microscopic slide with a coverslip. They were smoothly squashed (to splay them and produce a single cell layer) and submerged briefly in liquid nitrogen. Then, after removing coverslips, they were left out to dry at room temperature for one hour. To permeabilize the samples, the slides were immersed in 70% ethanol overnight on a rotary shaker prior to hybridization. The ethanol was evaporated at room temperature before washing the roots with MES.

SmFISH was used for the detection of MS2 repeats and endogenous *SPX1* mRNAs. The MS2 probe was made of a mix of 10 pre-labelled fluorescent oligos directed against 32xMS2 repeats [13]. Each oligo contains 2 to 4 molecules of Cy3 and hybridizes 4 times across 128xMS2 repeats, allowing the binding of 40 probes to each single RNA molecule. The set of *SPX1* probes was made of a mix of 24 fluorescent oligonucleotides carrying 2 to 3 Cy3

fluorophores and covering the entire SPX1 transcript including 5' and 3' UTR (Table S2). The pre-hybridization was performed in 1xSSC/40% formamide buffer for 15 min at room temperature. Hybridization was performed with 2 ng/µl probe and in 40% formamide for MS2, whereas for *SPX1* only 15% formamide was used. The smiFISH probe mix directed against the post-polyA region of the MS2 construct was made of 21 oligonucleotides (Table S2) and hybridized as previously described [51]. After addition of probes, samples were covered with a coverslip and remained overnight at 37°C as previously described [51]. For rinsing, after coverslip removal, root samples were washed twice during 45 min at 37°C with freshly prepared 1xSSC/40% formamide buffer and rinsed at room temperature with MES pH 5.8 buffer and dried. A drop of Prolong Diamond antifade mounting medium (Invitrogen) containing DAPI was added prior to observation. For long-term storage, slides were kept at -20°C.

Fluorescence imaging of fixed plants

SmFISH and MCP-GFP images were taken using either a spinning disk confocal or a wide field microscope. For spinning disk microscopy, we used a Dragonfly (Oxford instrument) equipped with four laser lines (405, 488, 561, 637 nm) and an ultrasensitive EMCCD camera (iXon Life 888, Andor) mounted on a Nikon Eclipse Ti2 microscope body, using a 40x, NA 1.3 Plan Fluor oil objective or a 60x, NA 1.4 Plan Apochromat oil objective coupled with a supplementary lens of 2x, using z-stacks with a 0.5 µm or 0.4 µm step. For wide field imaging, we used a Zeiss Axioimager Z1 wide-field upright microscope equipped with a camera sCMOS ZYLA 4.2 MP (Andor), using a 100x, NA 1.4 Plan Apochromat oil objective. For these z stacks, a step of 0.3 or 0.4 µm was used. Maximal image projections (MIP) were generated with ImageJ, and figures were realized using Adobe Photoshop and Illustrator. The

mosaic of Figure 3A is accessible with a viewer run with Imjoy[52]. Note that plant fixation and smFISH both reduced the GFP signals.

Analysis and quantifications of smFISH images

Quantification of the brightness of transcription sites was made with a modified version of HotSpot [40]. This is a user-friendly MatLab software that allows to quantify smFISH signals in very noisy images, unlike FISH-quant[53,54]. Briefly, the user can navigate in 2D or 3D bicolor images to manually select transcription sites and single RNAs, and the script finds the local maxima and fits 2D or 3D gaussians to the selected transcription spots. The images of single RNAs are averaged and also fitted to 2D or 3D gaussians, and the integrated intensity of the transcription sites are divided by the intensity of average of single RNAs, yielding the exact number of molecules present at transcription sites. In this work, quantifications were done in 2D on MIPs using 100-500 single RNA per image to generate the average. HotSpot is available on GitHub (https://github.com/muellerflorian/hotspot).

To calculate initiation rates, we assumed that initiation occurs at random with a constant rate. This produces a uniform distribution of RNA polymerases along the *SPX1* gene following arithmetic series. Because the MS2 and *SPX1* probes are distributed homogeneously along the corresponding pre-mRNAs, incomplete nascent RNAs are labelled with only a fraction of the probes. If one assumes that the pre-mRNAs immediately leave the transcription site once polymerases reach the 3'-end of the gene (in agreement with experimental data), the barycenter of the polymerase distribution is the middle of the gene, and the average brightness of a nascent pre-mRNA is thus half that of a full-length pre-mRNA. In this case, the number of polymerase on the gene, Npol, is thus twice the brightness of transcription sites, expressed in number of full-length pre-mRNA (noted TS_{RNA}). Assuming an elongation rate of 2kb/min, the time to transcribe the gene, t_{el}, is 42 s, and the average

initiation rate is Npol divided by t_{el}. If the pre-mRNA takes t_{proc} seconds to be 3'-end processed and released from the transcription site, then Npol is $TS_{RNA}*[2*t_{el}/(t_{el}+t_{proc})+ t_{proc}/(t_{el}+t_{proc})]$, and the initiation rate is Npol divided by $(t_{el}+t_{proc})$.

To analyze the distribution of distances separating active transcription sites within single nuclei, we computed for each nuclei all the distances between all the visible transcription sites. To simulate a random distribution of transcription sites, Arapidopsis nuclei were simulated as ellipses with a major axis length of 12 µm and a minor axis length of 6 µm, and we randomly selected points using a uniform distribution in the ellipse surface.

To measure total (n_{tot}), extrinsic (n_{ext}) and intrinsic (n_{int}) noise for cells with any number of alleles, we used an extension of the approaches previously developed [36,37]. For a population of cells with n alleles, we considered the brightness of the transcription sites of the n alleles, expressed in number of full-length pre-mRNA molecules, as n random variables. We computed the corresponding variance-covariance matrix of these n variables and defined n_{tot} as the root square of the mean of the variances given by the matrix diagonal, n_{ext} as the root square of the mean of the covariances obtained by the non-diagonal values of the matrix, and n_{int} as the root square of n_{tot}^2-n_{ext}^2. The error in n_{tot}, n_{int} and n_{ext} was estimated by randomly attributing each of the n transcription sites to the n alleles, calculating n_{tot}, n_{int} and n_{ext} and repeating this 100 times to calculate the standard deviation of the values obtained.

In Figure 2D, he number of expressing cells (i.e. cells having at least 20 RNA molecules in the nucleus or the cytoplasm), as well as the number of transcription site per cell (see Fig. 4C-D), was counted manually from 2D MIP smFISH images. The plot of Figure 4 were generated in R and incorporated in the figure using Adobe Illustrator.

Rootchips and *in vivo* live plants imaging experiments

For these experiments, we used brightest line obtained with *SPX1* promoter (the S and J lines). Transgenic seeds were germinated in conical cylinders produced from micropipette tips filled with -P agar and inserted into sterile -P agar plates. 5 to 7 day old Pi deficient seedlings were then transferred into a RootChips [22,38], grown vertically and fed with a Pi deficient nutritive solution at a low flow pressure until the root grew in the channel. For refeeding experiment, the nutritive solution was changed from –Pi to +Pi. Synaptored^{TM}C2 (5µg/mL, Ozyme) was added into the +P solution to detect the arrival time of Pi (defining t=0). In vivo movies were recorded with an Andor Dragonfly spinning disk mounted on a Nikon Eclipse Ti using 40x Plan-Apo water objective (1.15 NA; 0.6 mm DT). Z-stacks were made every 3 minutes with a scan size of 100-150µm (0.5µm step size; ~200 steps per Z-stack). The data was analyzed with the ImageJ software using the TrackMate plugin to track transcription sites on 2D MIPs. The intensity of *SPX1* transcription sites was assessed for several nuclei per sample. In each nucleus, the mean intensity of the nuclear background was subtracted to the maximum intensity of *SPX1* transcription site, and the resulting intensities were plotted against time.

610 **Figure Legend**

611

612 **Figure 1**: **identification of fast responsive transcripts regulated at transcriptional level**
613 **by phosphate resupply.**

614 (A) RTqPCRs of roots of seedlings grown for 7 days either in the presence of Phosphate
615 (+Pi), in the absence of Phosphate (-Pi), or in the absence of Phosphate for 7 days followed by
616 Phosphate resupply for 30 minutes (Re30) or 60 minutes (Re60). *EIF4A,* a translation
617 initiation factor known not to react to cordycepin addition was used as control[45]; n =2-3.

618 (B) Model depicting the transcriptional regulation by phosphate.

619 (C) RTqPCRs of roots of WT and *phr1/phl1* seedlings grown during 7 days under +Pi and –
620 Pi; n=2-3.

621 (D) RTqPCRs of roots of WT and *spx1/spx2* seedlings grown during 7 days under +Pi or -Pi,
622 and supplemented with Pi for 30 or 60 minutes; n=3-5.

623 (E) Kinetic of luminescence measurements in pUNI1::LUC transgenic seedlings between –Pi
624 and resupplied sample, value are relative to –Pi; n=5.

625 For all RTqPCR experiments *TUBULIN* was used as a housekeeping reference gene for
626 normalization. Values are $\log_{10}$ relative expression levels (REL) normalized to 1 for -Pi levels
627 at time zero represented. Different letters indicate significantly different means (SNK one-
628 way ANOVA, $p<0.05$, Rstudio). Error bar represent standard deviation and n is the number of
629 biological replicates used for RNA extraction.

630

631 **Figure 2: Validation of pSPX1::MS2x128 transgenic plants.**

632 (A) Principle of the MS2-MCP system. The transgene is under the control of the *SPX1*
633 promoter and synthesizes a reporter RNA bearing 128 MS2 stem-loops, which are recognized
634 by the MCP protein fused to a fluorescent marker (eGFP).

(B) Microscopy images of squashed root caps of the transgenic S line expressing pSPX1::MS2x128 and processed for smFISH with probes hybridizing to the MS2x128 sequence. Left: Pi depleted sample (-Pi) and zoomed over the boxed area in the middle panels. Right: sample grown on Pi rich medium (+Pi). Top: smFISH signals; bottom: smFISH signals colored in red and merged with Dapi (blue). Images are maximal projections of z-stacks (widefield microscopy). Scale bars: 40 µm (left and right panels), and 4 µm (middle panels). Transcription sites and single RNA molecules are indicated by orange and pink arrows, respectively.

(C) Legend as in B except that smFISH was performed with probes hybridizing against the endogenous *SPX1* mRNAs in WT squashed roots in the cap (right panel) and mature tissue (left panel). Scale bars: 4 µm.

(D) Bar plot depicting the number of cells expressing the endogenous *SPX1* mRNA (orange, WT plants), or the pSPX1::MS2x128 reporter RNA (blue, S plants) in root (data for root cap and mature root area are combined), with (+Pi) or without (-Pi) phosphate. Mean and standard deviation estimated from 12 fields of view for *SPX1* probes (n=300) and 23 for MS2 probes (n=3087). Expressing cells are defined here as cells having at least 20 RNA molecules in the nucleus or the cytoplasm.

Figure 3: imaging *SPX1* transcription in fixed plant tissues reveals allelic differences in the root cap and polyploid expression in mature tissue.

(A) Organization of Arabidopsis root, with the name of the various root parts and tissues overlayed on a microscopy mosaic image of a homozygous S plant with MCP-GFP (green) and DNA (blue). Inset: ploidy of the root tissue. Note that a viewer with a zoomable high resolution version of the mosaic can be accessed at https://imjoy.io/lite?plugin=muellerflorian/hani-ms2:hani-ms2-sample-3.

(B) Images are maximal image projections of z-stack from a root cap of a homozygous S plant grown without Pi and imaged by spinning disk microscopy in three colors. Left (and red in the Merge panel): smFISH signals obtained with probes against the MS2 repeat; middle (and green in the Merge panel): MCP-GFP signals. Blue: nuclei stained with Dapi. The bottom panels are zooms of the boxed area in Merge panel. Pink arrows: single RNA molecule; orange arrows: transcription sites. Scale bar: 100 µm (top panels) and 10 µm (bottom panels).

(C) Legend as in B, except that a mature part of the root is imaged. Note that images in A, B and C come from different plantlets.

Figure 4: quantitation of *SPX1* transcription in fixed cells gives insights into transcription dynamics, ploidy and intrinsic *vs.* extrinsic noise.

(A) Graph depicting the distribution of the brightness of active transcription sites for the endogenous *SPX1* gene (left), or the SPX1-MS2x128 reporter (right) both detected by smFISH. Brightness values are expressed in number of full-length RNA molecules (x-axis), and the y-axis represent the number of cells with these values.

(B) Model of *SPX1* transcription, based smFISH data labelling the endogenous *SPX1* mRNAs.

(C) Graph depicting the number of active transcription sites per cell for the SPX1-MS2x128 reporter detected by smFish on 4 plants (488 nuclei) for mature tissue and 3 plants (641 nuclei) for root cap. x-axis: number of active transcription sites per cell; y-axis: fraction of cells with these values. Orange bars: diploid root cap cells; blue bars: differentiated, polyploid cells. Error bars represent standard deviation.

(D) Graph depicting the number of active transcription sites per cell for the endogenous *SPX1* mRNA detected by smFish on 9 plants (300 nuclei) for mature and 3 plants (137 nuclei) for root cap. Legend as in C.

(E) Histogram depicting the distance distribution between active transcription sites in single cells, for the endogenous *SPX1* gene and for polyploid cells having 4 or more sites. Distances are expressed in µm (x-axis), and the y-axis represent the number of cells with these values. Pink curve: distance distribution obtained by simulating a random location of 8 spots within Arabidopsis nuclei.

(F) Image is a maximal image projection of a z-stack from a differentiated root cell labelled by smFISH with probes against the endogenous *SPX1* mRNA (widefield microcopy). Red: smFISH signals; blue: nucleus stained with Dapi. Scale bar: 5 microns.

(G) Graph depicting the correlation of activities of *SPX1* alleles, in cells having one or two active transcription sites. x-axis: number of molecules at the first transcription site; y-axis: number of molecules at the second transcription site.

(H) Graph depicting the levels of total, intrinsic and extrinsic noise for cells with either 2 active transcription sites (left), or 3-4 (right). Error bars represent the error estimated by bootstrapping (see Methods).

Figure 5: **combining microfluidic and MS2 technology reveals the fast transcriptional repression triggered by Pi supply in pSPX1::MS2x128 transgenic plants.**

(A) Principle of experiment combining RootChip microfluidic system with spinning disk microscopy to analyze the transcriptional response to Pi refeeding in real time.

(B) Image is a maximal image projection from a time-lapse movie recorded in 3D (200 z-planes), which displays MCP-GFP fluorescence in S plants at the start of Pi refeeding (t=0). Scale bar: 100 µm. Inset: identical image with a higher contrast to display the tissue structure.

(C) Images are maximal image projection from the time-lapse movie shown in B, taken at the indicated time points after Pi refeeding and displaying MCP-GFP fluorescence. Scale bar: 10 µm.

Figure 6: the SPX1 promoter generates bursts of activity in root cap cells grown at steady-state in absence of phosphate.

(A) Image is a maximal image projection from a time-lapse movie recorded in 3D (44 z-planes 600 nm apart), which displays MCP-GFP fluorescence in S plants. Scale bar: 20 µm.

(B and C) Images are maximal image projection (MIP) on XY (A) or XZ (B) axes from the time-lapse movie shown in A, taken at the indicated time points and displaying MCP-GFP fluorescence. Arrows pinpoint transcription sites where the signal remains constant (green), increases (blue) or turns off and then on (orange) during time-laps. Scale bar: 10 µm.

(D) Images are maximal image projection (MIP) on XY (A) or XZ (B) axes of a nucleus where transcription decreases at transcription site (orange arrow) and individual mRNA released can be seen (pink arrows). Scale bar: 5 µm.

Figure 7: **analysis of transcription site activity following Pi supply in pSPX1::MS2x128 S line transgenic plants.**

(A) Intensity of fluorescence signals at transcription sites in arbitrary units (a.u.), and recorded every 3 minutes after Pi refeeding, for cells exhibiting one or two active transcription sites (n=22) recorded in 14 mature root cells located 1mm above the root tip.

(B) Intensity of fluorescence of transcription sites over time, for 8 cells exhibiting two active transcription sites (plotted in same color).

(C) Normalized intensities of transcription sites over time, for the same cells as in A. Normalization is done according the value measured at t=0.

(D) Average normalized intensities of transcription site, for the 22 transcription sites shown in panels A and B (mean and standard deviation).

(E) Same average curve of normalized transcription site intensities as (D) obtained with independent plant samples.

(F) Average curve obtained by analysis of 67 transcription sites analyzed on 5 plants.

(G) Intensity of fluorescence signals at transcription sites in arbitrary units (a.u.), and recorded every 3 minutes for cells exhibiting one or two active transcription sites of plant supplied with Pi depleted nutrient solution, (n=14)

(H) Normalized intensities of transcription sites over time, for the same cells as in G. Normalization is done according the value measured at t=0. Standard deviation is provided (n=14).

Supplemental Figure 1: **identification of genes rapidly responding to Pi resupply.**

(A) List of the fastest genes (presenting a $|\text{Fold Change } (\text{Log}_2)| > 1$) common in all the replenish RNAseq points in roots (30, 60 and 180 min), accompanied with the values obtained in shoots. Their possible regulation by PHR1/PHL1 has also been tested: presence of P1BS box 3kb upstream or 3 Kb downstream, and misregulation in *phr1/phl1* double mutant (data from Bustos et al., 2010, or analyzed by RTqPCRs and labelled* (data not shown).

(B-C-D) RTqPCR analysis of the effect of Pi replenishing for different markers WT (B-C-D) or transgenic pSQD2::LUC (C) or p35S::SPX1-GFP (D) lines. In the p35S::SPX1-GFP line, repression triggers by Pi resupply does not affect SPX1-GFP transcript whereas SPX3 mRNA (close homologue of SPX1, identified as early responding genes in the S1A list) remains strongly regulated as observed in the WT background.

The X-axis legend refers for (B) to markers analyzed in the WT background, whereas for (C and D) it refers to genetic background used (WT or transgenic), markers analyzed (LUC, GFP, SPX3) are mentioned above the graphs.

TUBULIN was used as housekeeping gene. Values are $\log_{10}$ relative expression to -Pi levels (REL), which are normalized to 1; n=3-5. Different letters indicate significantly different means (SNK one-way ANOVA, $p<0.05$, Rstudio). Error bar represent standard deviation and n the number of biological replicates used for RNA extraction.

Supplemental Figure 2: implementation and validation of the MS2 system in plants.

(A) Moclo vectors adapted to the Golden Gate system and cloning strategy used to introduce the MS2 system into plants.

(B) Images are maximal image projections of microcopy images from Arabidopsis roots grown in Pi depleted medium and processed for smFISH with probes hybridizing against the endogenous *SPX1* mRNAs. Top: SmFISH signal; bottom: merge with Dapi (blue); right panels: zoom over the boxed area. Scale bars: 40 μm (left), and 4 μm (right). Pink arrows: single RNA molecules; orange arrows: transcription sites.

(C) Graph depicting the distribution of the brightness of active transcription sites for the endogenous *SPX1* gene, for cells having 1 or 2 transcription sites (yellow bars), or more than 3 (blue bars). Brightness values are expressed in number of RNA molecules (x-axis), and the y-axis represents the frequencies of these values. a.u.: arbitrary units.

Supplemental Figure 3: genetic and molecular analysis of selected lines (J, S) expressing the pSPX1:MS2x128 transgene.

(A) Segregation analysis of Kanamycine resistance in the T2 progeny. Seeds were germinated on Hoagland/2 medium supplemented with kanamycin (50 mg/l). (+) = growth, (-) = death. c^2

values are provided for theoretical segregation ratio (3:1). The critical value for a p level of 0.05 is 3.84).

(B) Molecular analysis by qPCR of T-DNA presence in the Col, S and J lines. Set of primers used are described in the Supplemental Table1 to amplify GFP, MCP and the SPX1 promoter (the only gene present in all lines). Values are presented as relative amounts (REL) normalized to S line (100%). The endogenous SPX1 gene was used as reference gene to normalize the DNA amount between samples.

Supplemental Figure 4: the RNA produced by the SPX::MS2x128 transgene is capped and polyadenylated.

RT-PCR amplification of the MS2x128 and endogenous SPX1 RNA after total RNA immunoprecipitation using m7G antibody (m7G-RIP). After RIP, RNAs were reverse-transcribed using oligo(dT) prior to PCR amplification. Sets of primers targeting transgene or endogenous gene were used. Wild-type (Col0) and two different transgenic lines (S and J) were used. As negative control, total RNAs were treated with pyrophosphatase to remove the cap prior to RIP experiment and RT-PCR. I : Input fraction. E : Eluate fraction. L : Ladder.

Supplemental Figure 5: MS2 smFISH in control Col0 plants and homozygous pSPX1:MS2x128 S line grown without Pi.

(A) Microscopy images of squashed root caps of Col0 (right two panels) and transgenic S line (left two panels), grown without Pi and processed for smFISH with probes hybridizing to the MS2x128 sequence. Top: smFISH signals; bottom: smFISH signals colored in red and merged with Dapi (blue). Images are maximal projections of z-stacks (widefield microscopy). Scale bars: 40 µm (1st and 3^{d} panels), and 4 µm (2^{d} and 4th panels, zooms corresponding to the

boxed area of the other panels). Transcription sites and single RNA molecules are indicated by orange and pink arrows, respectively.

(B) Legend as in A, but imaging was done on root mature tissue.

Supplemental Figure 6: SPX1 smFISH in Col0 and control spx1/spx2 mutant plants grown without Pi.

(A) Microscopy images of squashed root caps of Col0 (left two panels) and spx1/spx2 control plants (right two panels), grown without Pi and processed for smFISH with probes hybridizing to the SPX1 mRNA. Top: smFISH signals; bottom: smFISH signals colored in red and merged with Dapi (blue). Images are maximal projections of z-stacks (widefield microscopy). Scale bars: 40 µm (1^{st} and 3^{d} panels), and 4 µm (2^{d} and 4^{th} panels, zooms corresponding to the boxed area of the other panels). Transcription sites and single RNA molecules are indicated by orange and pink arrows, respectively.

(B) Legend as in A, but imaging was done on root mature tissue.

Supplemental Figure 7: imaging pUnicorn1::MS2x128 and pSPX1:MS2x128 J line in fixed plant tissues.

(A) Microscopy images of squashed mature tissue of the homozygous J line expressing pSPX1::MS2x128 grown without Pi and processed for smFISH with probes hybridizing to the MS2 sequence. Images are maximal image projections of z-stacks taken in three colors. Left (and red in the Merge panel): smFISH signals obtained with probes against the MS2 repeat; middle (and green in the Merge panel): MCP-GFP signals. Blue: nuclei stained with Dapi. The bottom panels are zooms of the boxed area in Merge panel. Orange arrows: transcription sites. Scale bars: 40 µm (top panels) and 4 µm (bottom panels).

(B) Legend as in B, except that a pUnicorn1::MS2x128 transgenic plant was imaged.

Supplemental Figure 8: combining microfluidics and MS2 technology reveals the fast transcriptional repression triggered by Pi supply in the S line.

(A) Image is a maximal image projection from a time-lapse movie recorded in 3D (200 z-planes) in the pSPX1::MS2x128 S line, and displays MCP-GFP fluorescence in plants at the start of Pi refeeding (t=0; set when the Synaptored dye is detected). Scale bar: 50 µm. Inset: identical image with a higher contrast to display the tissue structure.

(B and C) Images are maximal image projection from the time-lapse movie shown in A, taken at the indicated time points after Pi refeeding and displaying MCP-GFP fluorescence. Scale bar: 10 µm.

Supplemental Figure 9: number of active transcription sites before and following Pi resupply in the pSPX1::MS2x128 S line.

(A) During time lapse, the root is growing and moving in the microfluidic channel of the chip and some nuclei get out of focus. The blue curve depicts the number of nuclei still tracked at each time point (normalized to the initial number of nuclei; n_n=113). The orange curve indicated the number of active transcription sites detected in those nuclei, normalized to number of transcription sites present when the recording started (n_t=107).

(B) Biological replicates of (A) with n_n= 62, 66, 94, 81 and n_t= 49, 72, 45, 47 for plants 2 to 5 respectively.

Supplemental Figure 10: transcription site activity following Pi resupply in the pSPX1::MS2x128 J line transgenic plants.

(A) Normalized intensities of fluorescence signals at transcription sites over time, recorded every 3 minutes after Pi refeeding, for cells exhibiting one or two active transcription sites (n=16). Normalization is done according to the value measured at t=0.

(B) Average normalized intensities of transcription sites, for the 16 transcription sites shown in panel A (mean and standard deviation).

(C) Normalized intensities of fluorescence signals at transcription sites over time, and recorded every 3 minutes after Pi refeeding, for cells exhibiting one or two active transcription sites (n=13) in an independent plant than in (A). Normalization is done according to the value measured at t=0

(D) Average normalized intensities of transcription sites, for the 13 transcription sites shown in panel B (mean and standard deviation).

Supplemental Figure 11: transcription site activity upon continuous exposure to Pi depleted medium in pSPX1::MS2x128 S line transgenic plants.

(A) Maximal image projection from a time-lapse movie recorded in 3D (200 z-planes) and displaying MCP-GFP fluorescence in S plants in steady-state conditions (-Pi condition) from a mature root area. Scale bar: 100 µm. Inset: identical image with a higher contrast to display the tissue structure.

(B) The panels are zooms of the boxed area form (A) recorded in the time-lapse movie taken at the indicated time points and displaying MCP-GFP fluorescence. Scale bar: 20 µm.

Supplemental Figure 12: location of smFIH oligonucleotide probes on their respective targets RNA

(A) SPX1 mRNA.

(B) MS2x128 RNA.

878 (C) Post polyA region of the pSPX1::MS2x128 reporter gene.

879

880 **Supplementary Table 1**: **primer sequences used for RTqPCR and PCR reaction.**

881

882 **Supplementary Table 2: primer sequences for smFISH experiment.**

883 (A) Primers used to detect *SPX1* mRNA. Cy3 fluorescent dye is grafted on amino-modified

884 uridine analogue C6dT (labelled X on the sequence).

885 (B) Primers used in smiFISH to detect the post polyA region of the pSPX1::MS2x128

886 transcripts.

887 (C) Primers used to detect MS2x128 transcripts.

888

889 **Movie 1 and 2: bursting activity of the pSPX1::MS2x128 reporter**

890 Movie of root cap cells of Arabidopsis S line expressing pSPX1::MS2x128 and MCP-GFP,

891 and continuously grown without Pi. Maximal image projection (XY and XZ) are from a time-

892 lapse movie recorded in 3D (44 z-planes). Time (in min) is indicated. Movie 1 illustrates gene

893 bursting while Movie 2 illustrates the release of single RNAs in the nucleoplasm when

894 promoter activity stochastically turns off when a burst ends.

895

896 **Movies 3 to 8: Transcriptional repression of the pSPX1::MS2x128 reporter triggered by**

897 **Pi resupply.**

898 Movie of root cells of Arabidopsis S (2 to 7) and J (8) line transformed with

899 pSPX1::MS2x128 and MCP-GFP, after receiving a Pi rich solution at time t=0 min. Maximal

900 image projection from a time-lapse movie recorded in 3D (200 z-planes). Acquisitions lasted

901 39 min for Movies 3 and Movie 4 (Movie 4 zooms on few cells cropped from Movie 3), 54

902 min for Movie 5 to Movie 7 (Movies 6 and 7 are magnifications deriving from Movie 5), and
903 48 min for Movie 7.
904
905 **Acknowledgements**
906 S.H. was supported by a PhD fellowship from the CEA and PACA region, ANR Reglisse 13-
907 ADAP-008 fellowship and CEA DRF impulsion program with FOSSI project supported EM,
908 LC, LN, MCT, PD. Additional grant support were also received by HJ from CEA-Enhanced
909 Eurotalent and ANR PhlowZ 19-CE-13-0007. We thank Heliobiotech platform for the access
910 to their RTqPCR machine. We thank Dr E. Basyuk for her help with the MS2 plasmids, Dr L.
911 Laplaze and Dr G. Desbrosses for providing access to the growth chambers of IRD and
912 Montpellier University. We thank Dr. O. Radulescu for his help with calculating total,
913 extrinsic and intrinsic noise for an undefined number of alleles; Dr T. Desnos and C. Mercier
914 for their assistance on Figures drawing and Dr S. Kanno and Dr H. Garcia for critical reading
915 of the manuscript. We express our gratitude to the Dr J.M. Escudier for the synthesis of the
916 SPX1 set of fluorescent probes.
917 We acknowledge the MRI imaging facility (belonging to the National Infrastructure France-
918 BioImaging supported by the French National Research Agency, ANR-10-INBS-04), and the
919 ZoOM platform (supported by the Région Provence Alpes Côte d'Azur, the Conseil General
920 of Bouches du Rhône, the French Ministry of Research, the Centre National de la Recherche
921 Scientifique and the Commissariat à l'Energie Atomique et aux Energies Alternatives).
922
923 **Author contributions**
924 E.B. provided MS2 and MCP original constructs and LN conceived the experiments. L.C.,
925 S.H., P.D. performed all the experiments under LN supervision for physiological part and EB
926 supervision for cell biology. RNA seq data were produced by D.S. and J.W. and analyzed by

L.N., L.C. M-C.T. and E.M. Luminescence experiments were performed by N.P. under H.J. supervision. H.J. also implemented microfluidic technique in the SAVE team. Manuscript was written by LN and EB with help from S.H., P.D. and L.C.

Declaration of Interests

The authors declare no competing interests.

Bibliography

1 Lopez-Maury, L., Marguerat, S. & Bahler, J. Tuning gene expression to changing environments: from rapid responses to evolutionary adaptation. *Nature reviews. Genetics* **9**, 583-593, doi:10.1038/nrg2398 (2008).

2 Birnbaum, K. *et al.* A gene expression map of the Arabidopsis root. *Science* **302**, 1956-1960 (2003).

3 Balleza, E., Kim, J. M. & Cluzel, P. Systematic characterization of maturation time of fluorescent proteins in living cells. *Nature methods* **15**, 47-51, doi:10.1038/nmeth.4509 (2018).

4 Sorenson, R. S., Deshotel, M. J., Johnson, K., Adler, F. R. & Sieburth, L. E. Arabidopsis mRNA decay landscape arises from specialized RNA decay substrates, decapping-mediated feedback, and redundancy. *Proc Natl Acad Sci U S A* **115**, E1485-E1494, doi:10.1073/pnas.1712312115 (2018).

5 Narsai, R. *et al.* Genome-wide analysis of mRNA decay rates and their determinants in Arabidopsis thaliana. *Plant Cell* **19**, 3418-3436, doi:10.1105/tpc.107.055046 (2007).

6 Kollist, H. *et al.* Rapid Responses to Abiotic Stress: Priming the Landscape for the Signal Transduction Network. *Trends Plant Sci* **24**, 25-37, doi:10.1016/j.tplants.2018.10.003 (2019).

7 Bertrand, E. *et al.* Localization of ASH1 mRNA particles in living yeast. *Molecular cell* **2**, 437-445, doi:10.1016/s1097-2765(00)80143-4 (1998).

8 Fusco, D. *et al.* Single mRNA molecules demonstrate probabilistic movement in living mammalian cells. *Curr Biol* **13**, 161-167 (2003).

9 Boireau, S. *et al.* The transcriptional cycle of HIV-1 in real-time and live cells. *The Journal of cell biology* **179**, 291-304, doi:10.1083/jcb.200706018 (2007).

10 Lucas, T. *et al.* Live imaging of bicoid-dependent transcription in Drosophila embryos. *Curr Biol* **23**, 2135-2139, doi:10.1016/j.cub.2013.08.053 (2013).

11 Chao, J. A., Patskovsky, Y., Almo, S. C. & Singer, R. H. Structural basis for the coevolution of a viral RNA-protein complex. *Nature structural & molecular biology* **15**, 103-105, doi:10.1038/nsmb1327 (2008).

12 Pichon, X., Lagha, M., Mueller, F. & Bertrand, E. A Growing Toolbox to Image Gene Expression in Single Cells: Sensitive Approaches for Demanding Challenges. *Molecular cell* **71**, 468-480, doi:10.1016/j.molcel.2018.07.022 (2018).

13 Tantale, K. *et al.* A single-molecule view of transcription reveals convoys of RNA polymerases and multi-scale bursting. *Nature communications* **7**, 12248, doi:10.1038/ncomms12248 (2016).
14 Misson, J. *et al.* A genome-wide transcriptional analysis using Arabidopsis thaliana Affymetrix gene chips determined plant responses to phosphate deprivation. *Proc Natl Acad Sci U S A* **102**, 11934-11939 (2005).
15 Thibaud, M. C. *et al.* Dissection of local and systemic transcriptional responses to phosphate starvation in Arabidopsis. *Plant J* **64**, 775-789, doi:10.1111/j.1365-313X.2010.04375.x (2010).
16 Rubio, V. *et al.* A conserved MYB transcription factor involved in phosphate starvation signaling both in vascular plants and in unicellular algae. *Genes & development* **15**, 2122-2133 (2001).
17 Bustos, R. *et al.* A central regulatory system largely controls transcriptional activation and repression responses to phosphate starvation in Arabidopsis. *PLoS Genet* **6**, e1001102, doi:10.1371/journal.pgen.1001102 (2010).
18 Puga, M. I. *et al.* SPX1 is a phosphate-dependent inhibitor of PHOSPHATE STARVATION RESPONSE 1 in Arabidopsis. *Proc Natl Acad Sci U S A* **111**, 14947-14952, doi:10.1073/pnas.1404654111 (2014).
19 Wang, Z. *et al.* Rice SPX1 and SPX2 inhibit phosphate starvation responses through interacting with PHR2 in a phosphate-dependent manner. *Proc Natl Acad Sci U S A* **111**, 14953-14958, doi:10.1073/pnas.1404680111 (2014).
20 Zhu, J. *et al.* Two bifunctional inositol pyrophosphate kinases/phosphatases control plant phosphate homeostasis. *eLife* **8**, doi:10.7554/eLife.43582 (2019).
21 Wild, R. *et al.* Control of eukaryotic phosphate homeostasis by inositol polyphosphate sensor domains. *Science* **352**, 986-990, doi:10.1126/science.aad9858 (2016).
22 Grossmann, G. *et al.* The RootChip: An Integrated Microfluidic Chip for Plant Science. *Plant Cell*, doi:10.1105/tpc.111.092577 (2011).
23 Misson, J., Thibaud, M. C., Bechtold, N., Raghothama, K. & Nussaume, L. Transcriptional regulation and functional properties of Arabidopsis Pht1;4, a high affinity transporter contributing greatly to phosphate uptake in phosphate deprived plants. *Plant Mol Biol* **55**, 727-741, doi:10.1007/s11103-004-1965-5 (2004).
24 Tutucci, E. *et al.* An improved MS2 system for accurate reporting of the mRNA life cycle. *Nature methods* **15**, 81-89, doi:10.1038/nmeth.4502 (2018).
25 Engler, C., Gruetzner, R., Kandzia, R. & Marillonnet, S. Golden gate shuffling: a one-pot DNA shuffling method based on type IIs restriction enzymes. *PloS one* **4**, e5553, doi:10.1371/journal.pone.0005553 (2009).
26 Grefen, C. *et al.* A ubiquitin-10 promoter-based vector set for fluorescent protein tagging facilitates temporal stability and native protein distribution in transient and stable expression studies. *Plant J* **64**, 355-365, doi:10.1111/j.1365-313X.2010.04322.x (2010).
27 Duncan, S., Olsson, T. S. G., Hartley, M., Dean, C. & Rosa, S. A method for detecting single mRNA molecules in Arabidopsis thaliana. *Plant methods* **12**, 13, doi:10.1186/s13007-016-0114-x (2016).
28 Duan, K. *et al.* Characterization of a sub-family of Arabidopsis genes with the SPX domain reveals their diverse functions in plant tolerance to phosphorus starvation. *Plant J* **54** 965–975 (2008).

29 Bhosale, R. *et al.* A Spatiotemporal DNA Endoploidy Map of the Arabidopsis Root Reveals Roles for the Endocycle in Root Development and Stress Adaptation. *Plant Cell* **30**, 2330-2351, doi:10.1105/tpc.17.00983 (2018).
30 Levsky, J. M., Shenoy, S. M., Pezo, R. C. & Singer, R. H. Single-cell gene expression profiling. *Science* **297**, 836-840, doi:10.1126/science.1072241 (2002).
31 Femino, A. M., Fay, F. S., Fogarty, K. & Singer, R. H. Visualization of single RNA transcripts in situ. *Science* **280**, 585-590, doi:10.1126/science.280.5363.585 (1998).
32 Zhu, J., Liu, M., Liu, X. & Dong, Z. RNA polymerase II activity revealed by GRO-seq and pNET-seq in Arabidopsis. *Nat Plants* **4**, 1112-1123, doi:10.1038/s41477-018-0280-0 (2018).
33 Hetzel, J., Duttke, S. H., Benner, C. & Chory, J. Nascent RNA sequencing reveals distinct features in plant transcription. *Proc Natl Acad Sci U S A* **113**, 12316-12321, doi:10.1073/pnas.1603217113 (2016).
34 Furlong, E. E. M. & Levine, M. Developmental enhancers and chromosome topology. *Science* **361**, 1341-1345, doi:10.1126/science.aau0320 (2018).
35 Garcia, H. G., Tikhonov, M., Lin, A. & Gregor, T. Quantitative imaging of transcription in living Drosophila embryos links polymerase activity to patterning. *Curr Biol* **23**, 2140-2145, doi:10.1016/j.cub.2013.08.054 (2013).
36 Alamos, S., Reimer, A., Niyogi, K. K. & Garcia, H. G. Quantitative imaging of RNA polymerase II activity in plants reveals the single-cell basis of tissue-wide transcriptional dynamics. *bioRxiv* (2020).
37 Elowitz, M. B., Levine, A. J., Siggia, E. D. & Swain, P. S. Stochastic gene expression in a single cell. *Science* **297**, 1183-1186, doi:10.1126/science.1070919 (2002).
38 Guichard, M., Bertran Garcia de Olalla, E., Stanley, C. E. & Grossmann, G. Microfluidic systems for plant root imaging. *Methods Cell Biol* **160**, 381-404, doi:10.1016/bs.mcb.2020.03.012 (2020).
39 Bayle, V. *et al.* Arabidopsis thaliana High-Affinity Phosphate Transporters Exhibit Multiple Levels of Posttranslational Regulation. *Plant Cell* **23**, 1523-1535, doi:tpc.110.081067 [pii]
10.1105/tpc.110.081067 (2011).
40 Pichon, X. *et al.* Visualization of single endogenous polysomes reveals the dynamics of translation in live human cells. *The Journal of cell biology* **214**, 769-781, doi:10.1083/jcb.201605024 (2016).
41 Pena, E. J. & Heinlein, M. RNA transport during TMV cell-to-cell movement. *Frontiers in plant science* **3**, 193, doi:10.3389/fpls.2012.00193 (2012).
42 Kanno, S. *et al.* A novel role for the root cap in phosphate uptake and homeostasis. *eLife* **5**, doi:10.7554/eLife.14577 (2016).
43 Schubert, V., Berr, A. & Meister, A. Interphase chromatin organisation in Arabidopsis nuclei: constraints versus randomness. *Chromosoma* **121**, 369-387, doi:10.1007/s00412-012-0367-8 (2012).
44 Hanchi, M. *et al.* The Phosphate Fast-Responsive Genes PECP1 and PPsPase1 Affect Phosphocholine and Phosphoethanolamine Content. *Plant Physiology* **176**, 2943-2962, doi:10.1104/pp.17.01246 (2018).
45 Gutierrez, R. A., Ewing, R. M., Cherry, J. M. & Green, P. J. Identification of unstable transcripts in Arabidopsis by cDNA microarray analysis: rapid decay is associated with a group of touch- and specific clock-controlled genes. *Proc Natl Acad Sci U S A* **99**, 11513-11518, doi:10.1073/pnas.152204099 (2002).

46 Sarrobert, C. *et al.* Identification of an Arabidopsis thaliana mutant accumulating threonine resulting from mutation in a new dihydrodipicolinate synthase gene. *Plant J* **24**, 357-367. (2000).
47 Secco, D. *et al.* Stress induced gene expression drives transient DNA methylation changes at adjacent repetitive elements. *eLife* **4**, doi:10.7554/eLife.09343 (2015).
48 Godon, C. *et al.* Under phosphate starvation conditions, Fe and Al trigger accumulation of the transcription factor STOP1 in the nucleus of Arabidopsis root cells. *Plant J* **99**, 937-949, doi:10.1111/tpj.14374 (2019).
49 Pandolfini, L. *et al.* METTL1 Promotes let-7 MicroRNA Processing via m7G Methylation. *Molecular cell* **74**, 1278-1290 e1279, doi:10.1016/j.molcel.2019.03.040 (2019).
50 Harrison, S. J. *et al.* A rapid and robust method of identifying transformed Arabidopsis thaliana seedlings following floral dip transformation. *Plant methods* **2**, 19, doi:10.1186/1746-4811-2-19 (2006).
51 Tsanov, N. *et al.* smiFISH and FISH-quant - a flexible single RNA detection approach with super-resolution capability. *Nucleic acids research* **44**, e165, doi:10.1093/nar/gkw784 (2016).
52 Ouyang, W., Mueller, F., Hjelmare, M., Lundberg, E. & Zimmer, C. ImJoy: an open-source computational platform for the deep learning era. *Nature methods* **16**, 1199-1200, doi:10.1038/s41592-019-0627-0 (2019).
53 Mueller, F. *et al.* FISH-quant: automatic counting of transcripts in 3D FISH images. *Nature methods* **10**, 277-278, doi:10.1038/nmeth.2406 (2013).
54 Dufrene, Y. F., Martinez-Martin, D., Medalsy, I., Alsteens, D. & Muller, D. J. Multiparametric imaging of biological systems by force-distance curve-based AFM. *Nature methods* **10**, 847-854, doi:10.1038/nmeth.2602 (2013).

Figure 1

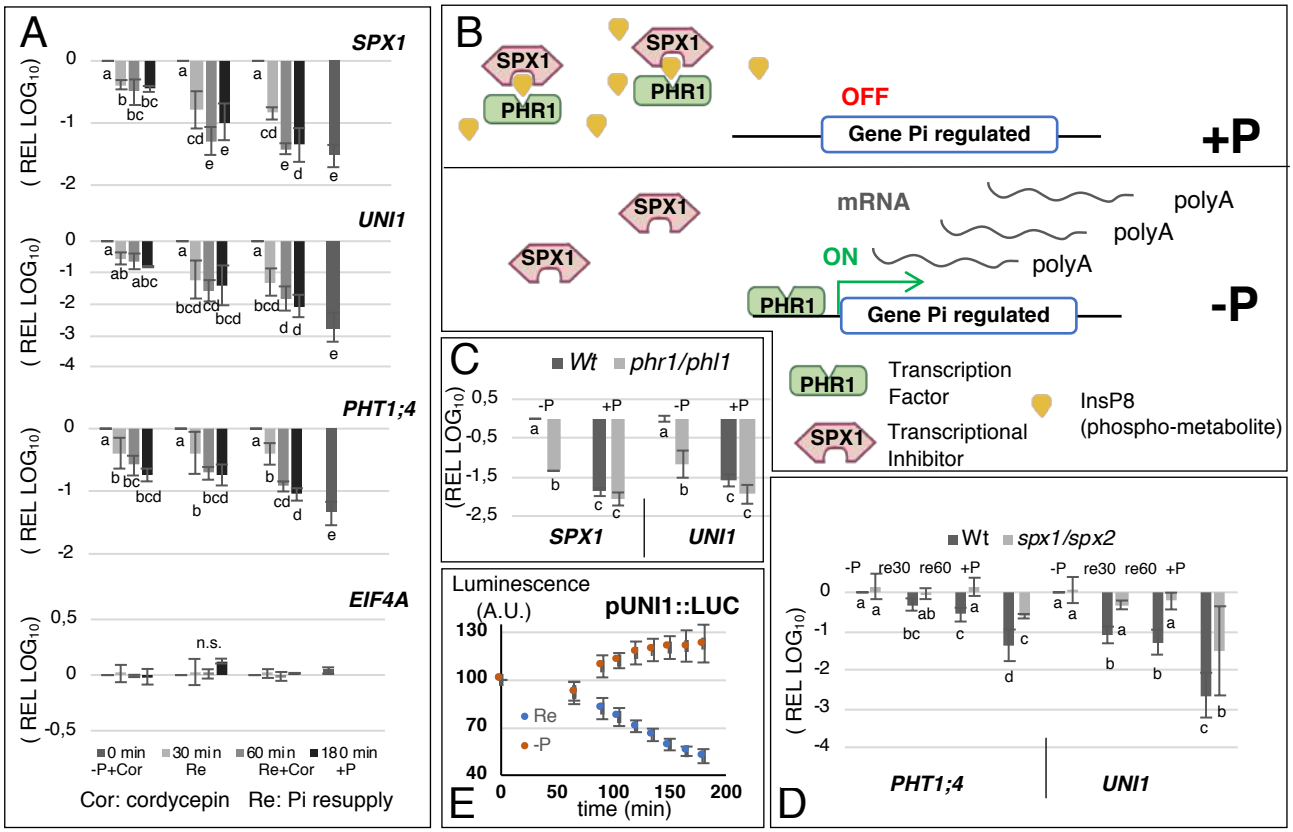
A
SPX1
UNI1
PHT1;4
EIF4A
(REL LOG10)
n.s.
0 min
-P+Cor
30 min
Re
60 min
Re+Cor
180 min
+P
Cor: cordycepin
Re: Pi resupply
B
SPX1
PHR1
OFF
Gene Pi regulated
+P
mRNA
polyA
ON
-P
Transcription Factor
Transcriptional Inhibitor
InsP8 (phospho-metabolite)
C
Wt
phr1/phl1
(REL LOG10)
-P
+P
SPX1
UNI1
E
Luminescence (A.U.)
pUNI1::LUC
Re
-P
time (min)
D
Wt
spx1/spx2
re30
re60
PHT1;4
UNI1

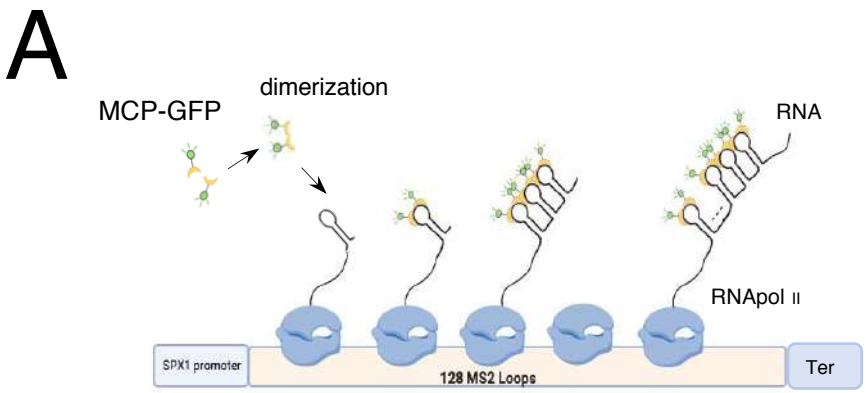
A
MCP-GFP
dimerization
RNA
RNApol II
SPX1 promoter
128 MS2 Loops
Ter

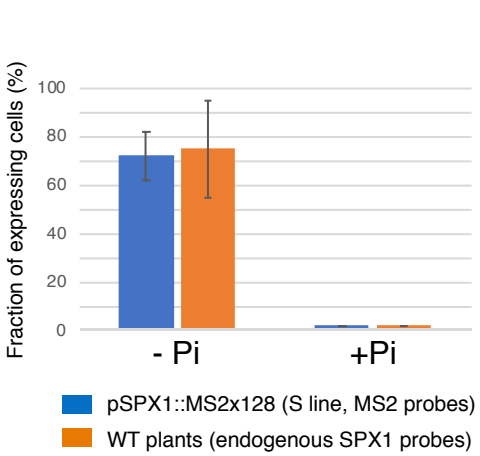
D
Fraction of expressing cells (%)
100
80
60
40
20
0
- Pi
+Pi
pSPX1::MS2x128 (S line, MS2 probes)
WT plants (endogenous SPX1 probes)

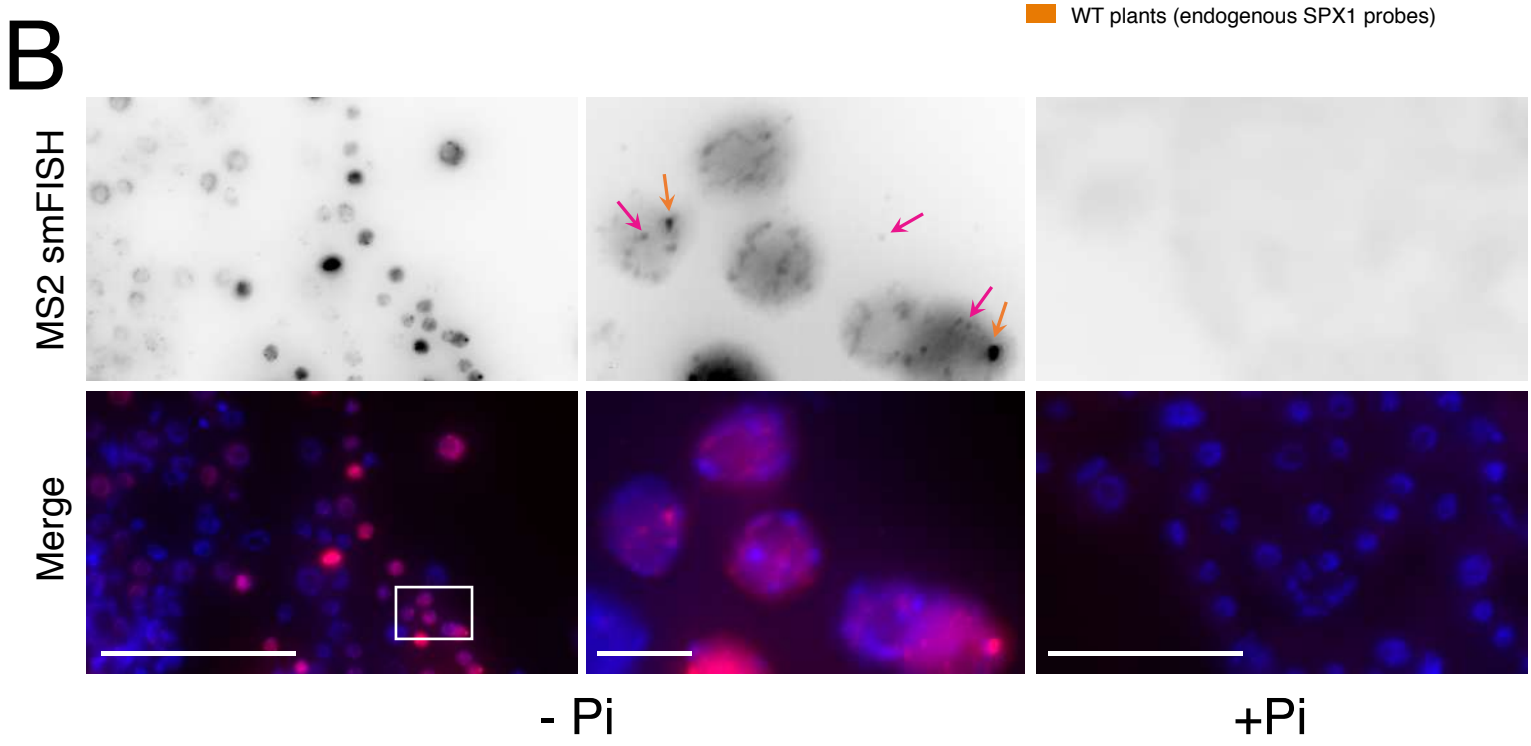
B
MS2 smFISH
Merge
- Pi
+Pi

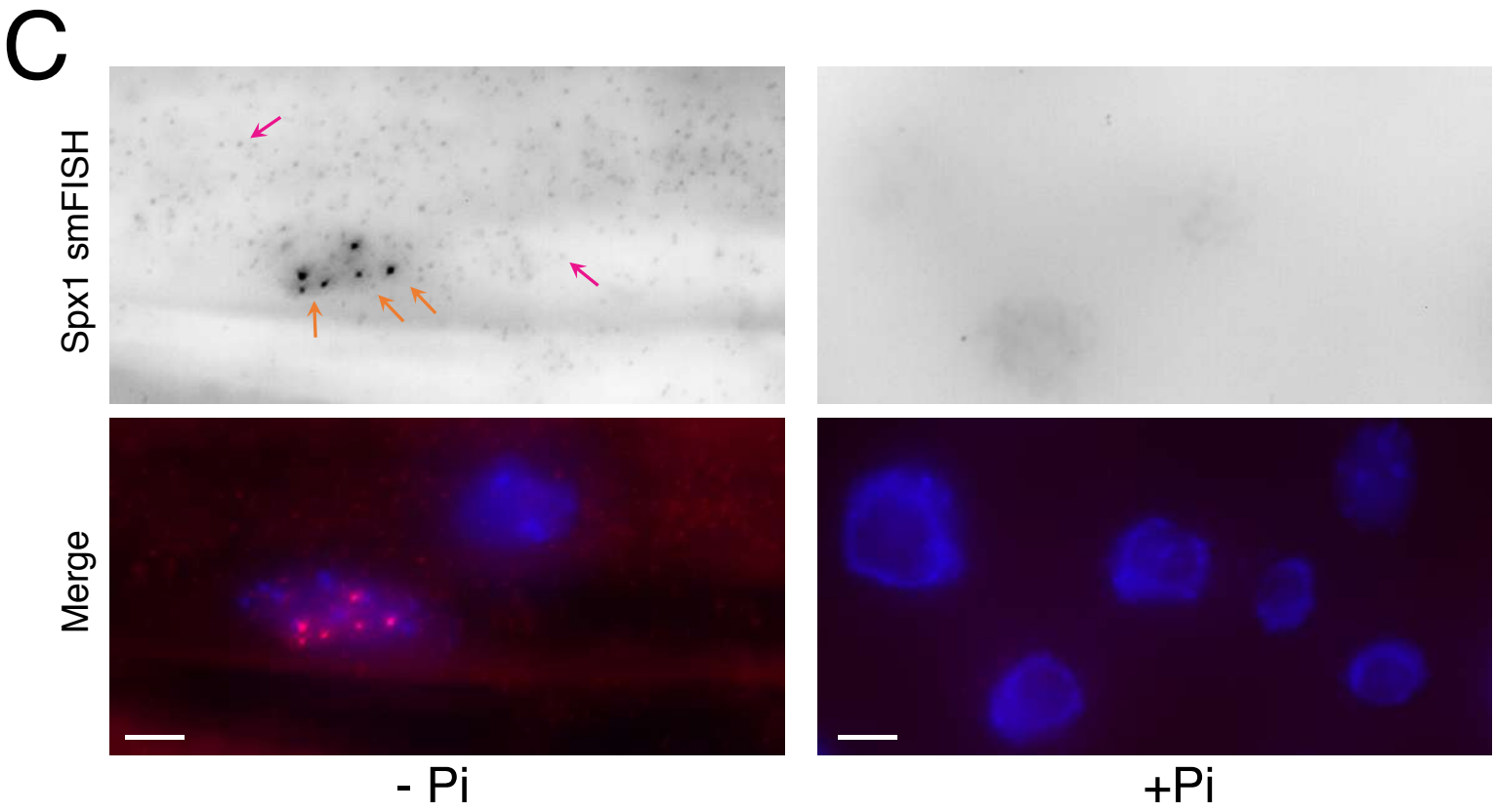
C
Spx1 smFISH
Merge
- Pi
+Pi

Figure 2

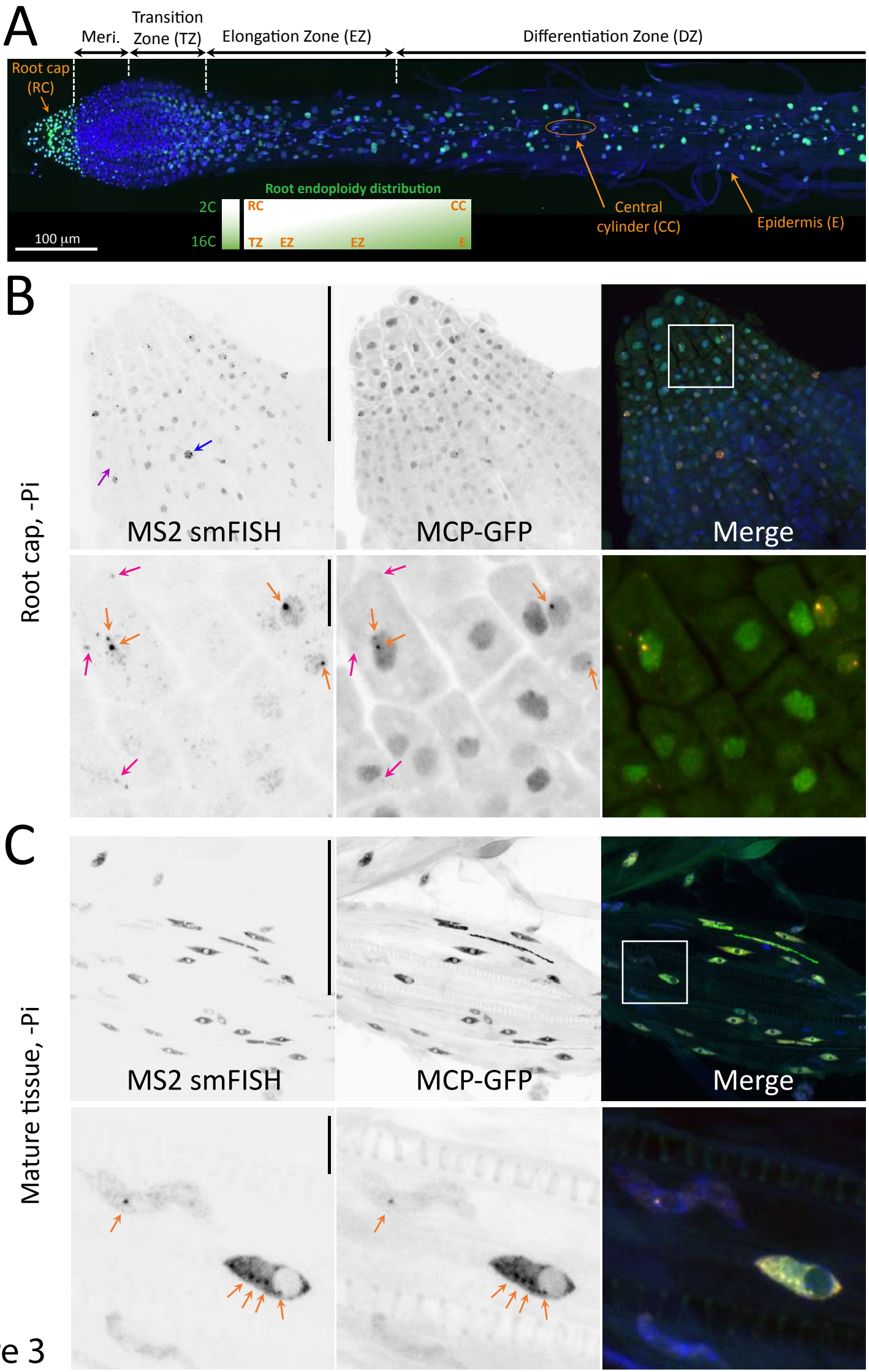
A
Meri.
Transition Zone (TZ)
Elongation Zone (EZ)
Differentiation Zone (DZ)
Root cap (RC)
Root endoploidy distribution
2C
16C
RC
CC
TZ
EZ
EZ
E
Central cylinder (CC)
Epidermis (E)
100 µm
B
Root cap, -Pi
MS2 smFISH
MCP-GFP
Merge
C
Mature tissue, -Pi
MS2 smFISH
MCP-GFP
Merge

Figure 3

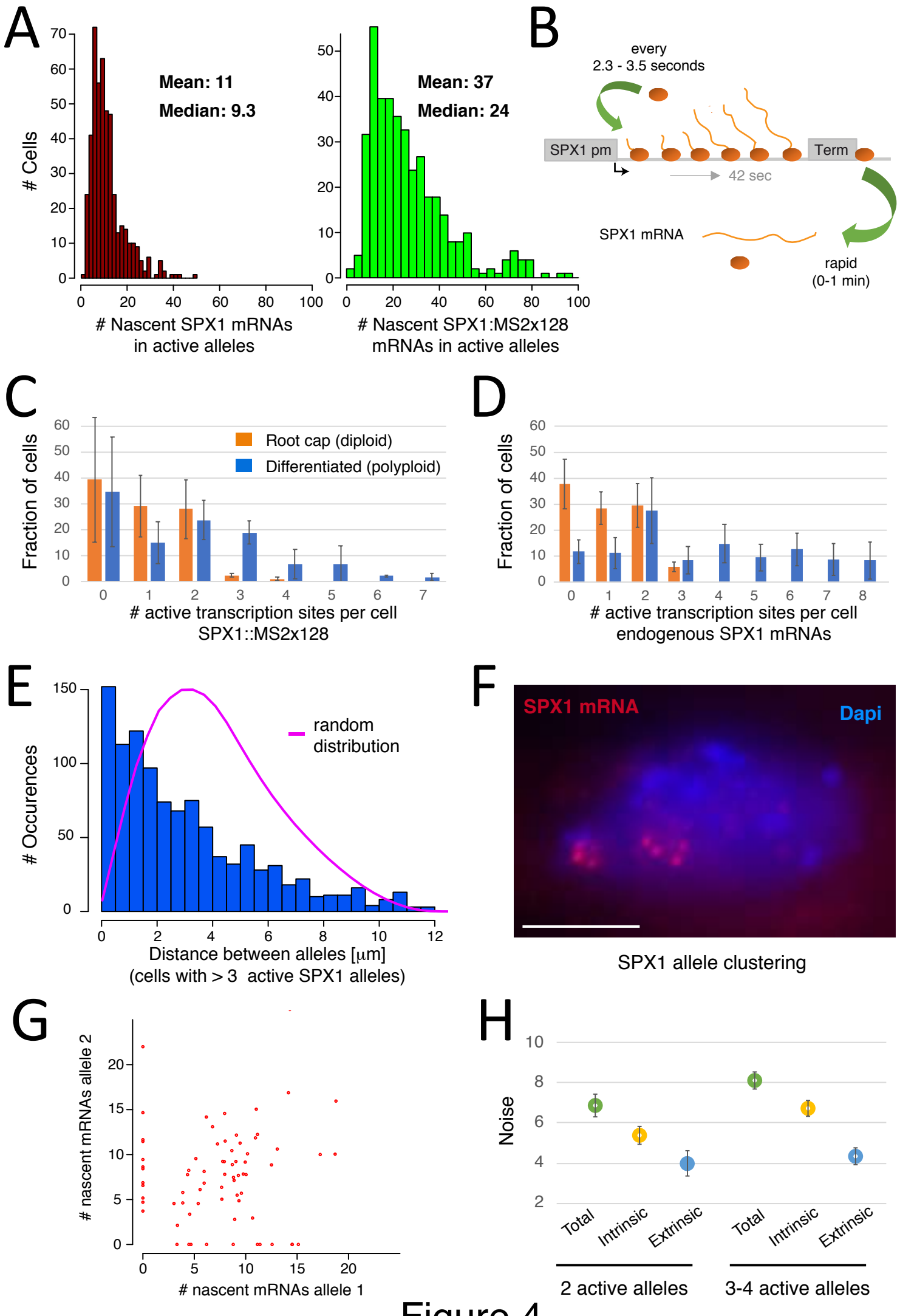
A
Cells
Mean: 11
Median: 9.3
Nascent SPX1 mRNAs in active alleles
Mean: 37
Median: 24
Nascent SPX1:MS2x128 mRNAs in active alleles
B
every 2.3 - 3.5 seconds
SPX1 pm
Term
42 sec
SPX1 mRNA
rapid (0-1 min)
C
Fraction of cells
Root cap (diploid)
Differentiated (polyploid)
active transcription sites per cell SPX1::MS2x128
D
Fraction of cells
active transcription sites per cell endogenous SPX1 mRNAs
E
Occurences
random distribution
Distance between alleles [μm] (cells with > 3 active SPX1 alleles)
F
SPX1 mRNA
Dapi
SPX1 allele clustering
G
nascent mRNAs allele 2
nascent mRNAs allele 1
H
Noise
Total
Intrinsic
Extrinsic
2 active alleles
3-4 active alleles

Figure 4

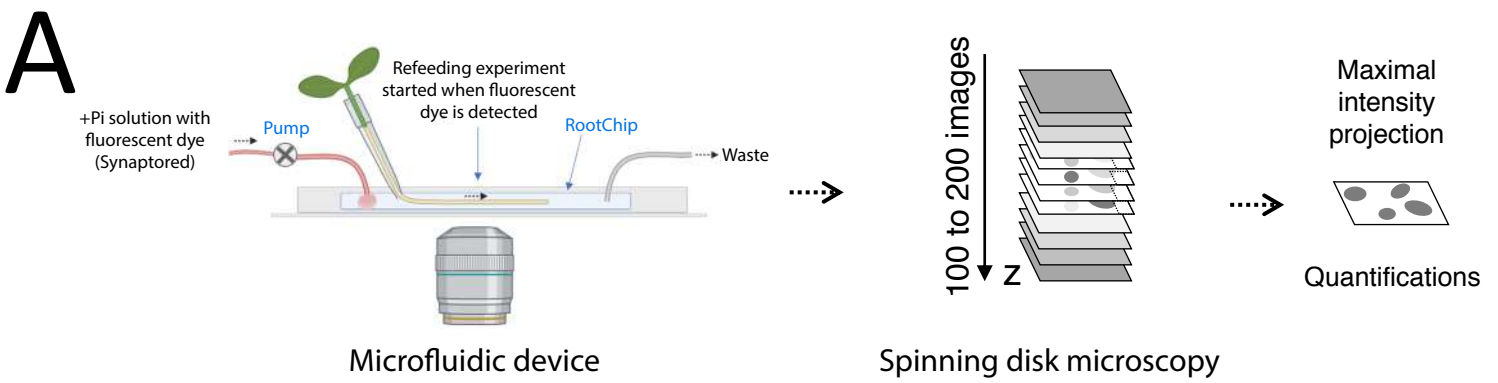
A
+Pi solution with fluorescent dye (Synaptored)
Pump
Refeeding experiment started when fluorescent dye is detected
RootChip
Waste
Microfluidic device
100 to 200 images
z
Spinning disk microscopy
Maximal intensity projection
Quantifications

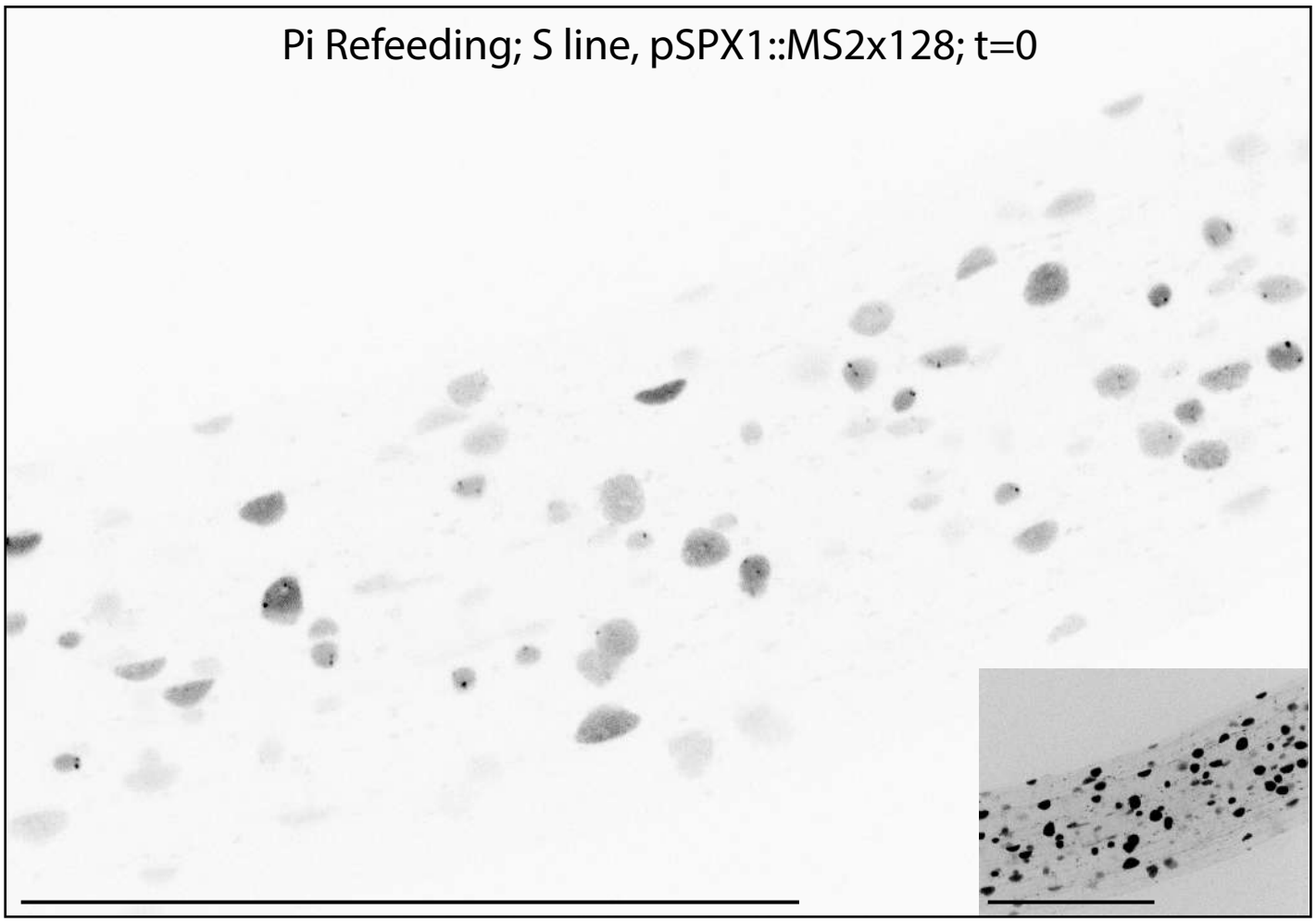
B
Pi Refeeding; S line, pSPX1::MS2x128; t=0

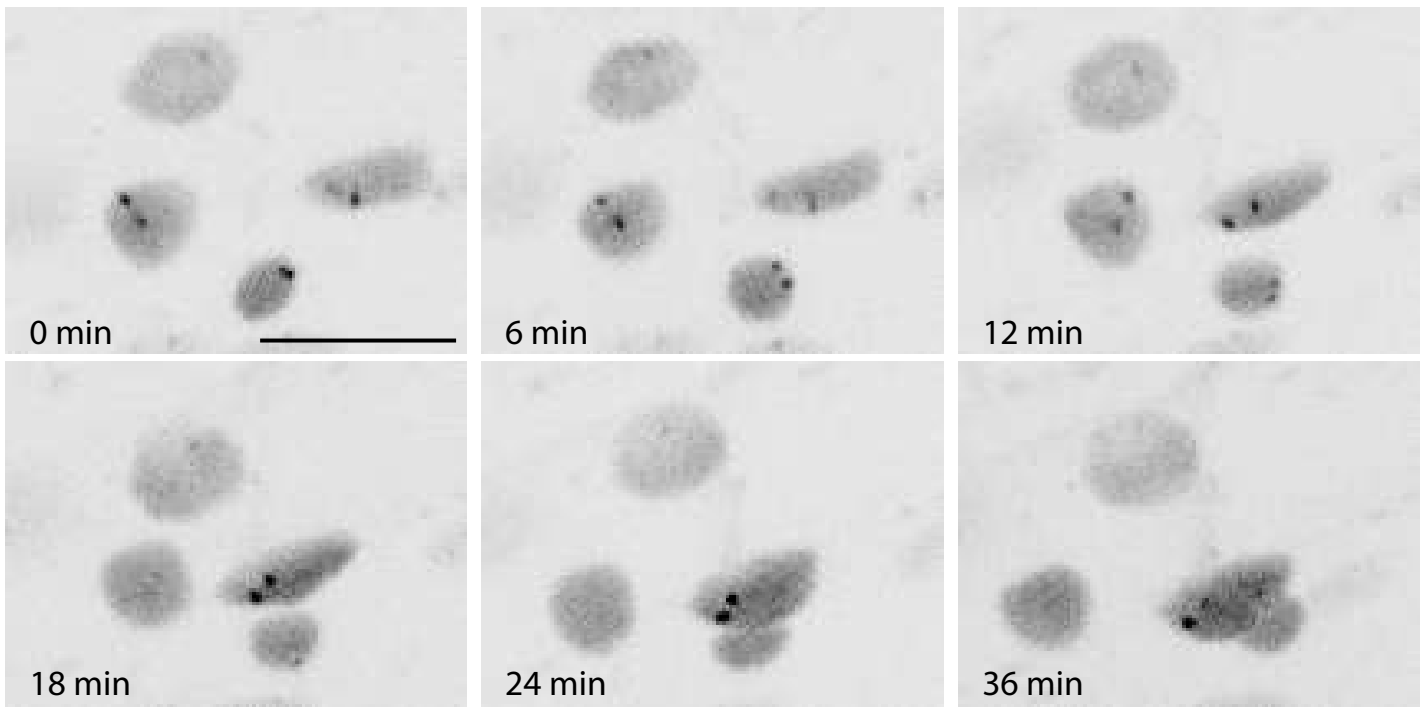
C
0 min
6 min
12 min
18 min
24 min
36 min

Figure 5

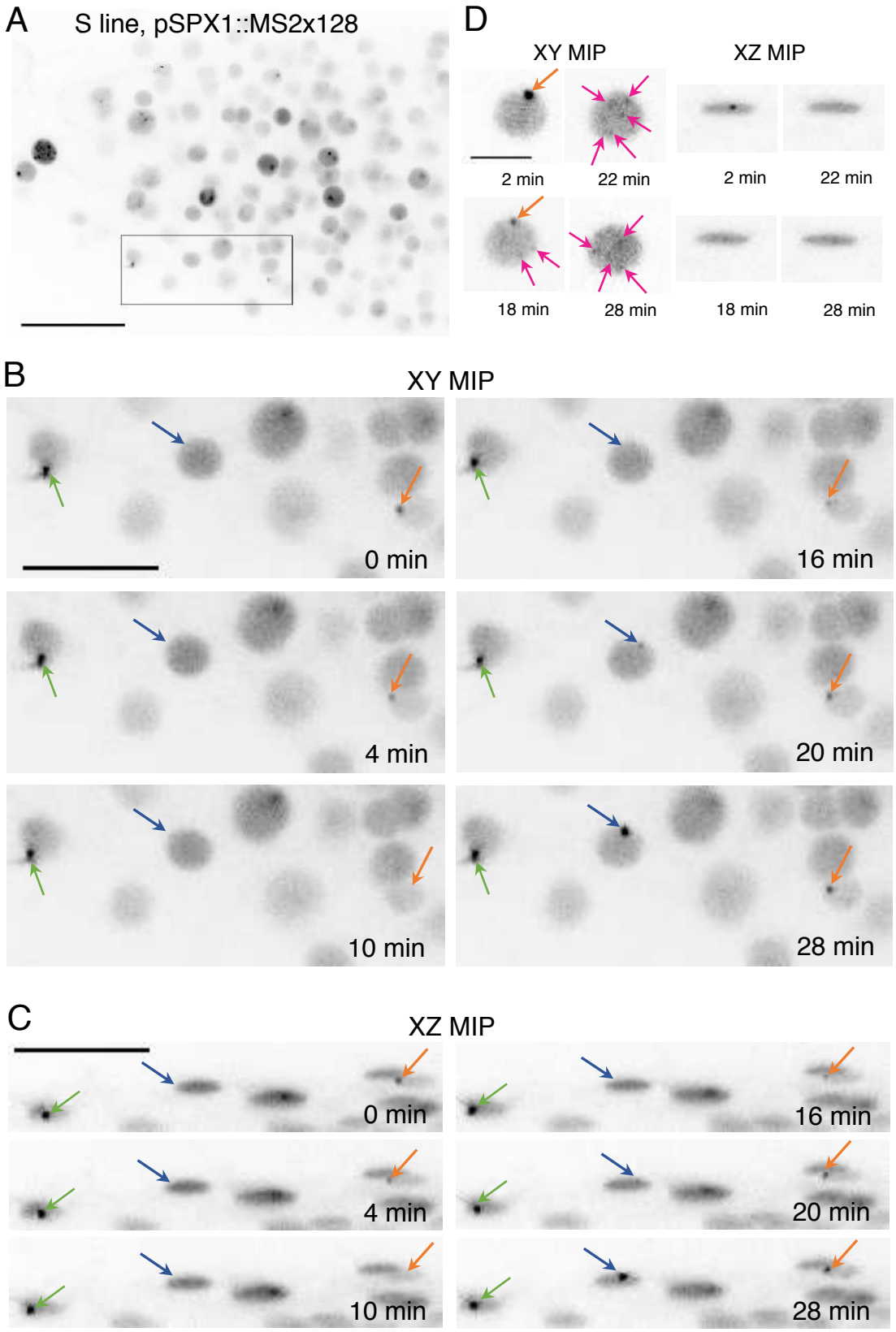
A
S line, pSPX1::MS2x128
D
XY MIP
XZ MIP
2 min
22 min
2 min
22 min
18 min
28 min
18 min
28 min
B
XY MIP
0 min
16 min
4 min
20 min
10 min
28 min
C
XZ MIP
0 min
16 min
4 min
20 min
10 min
28 min

Figure 6

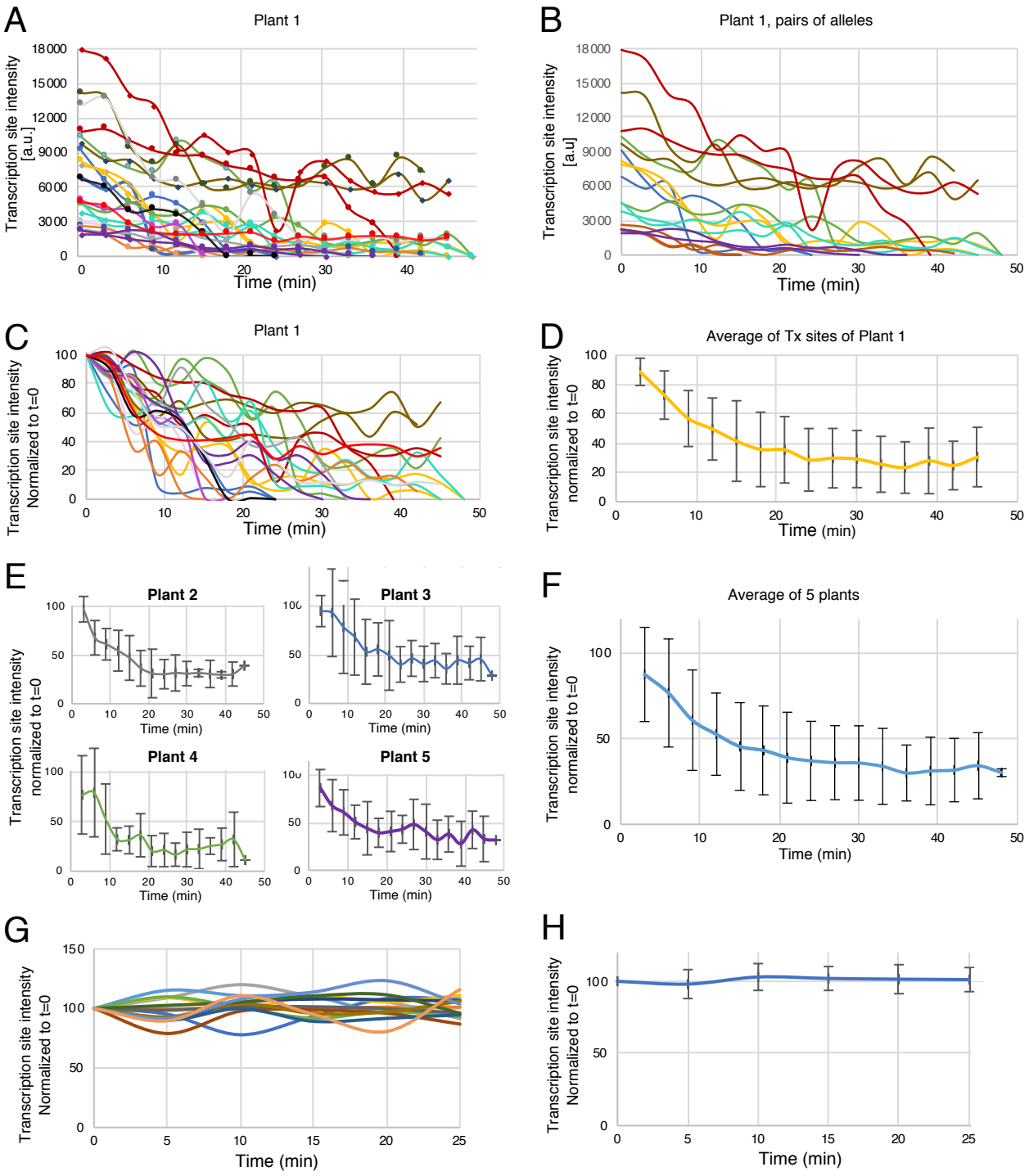

S line, pSPX1::MS2x128

Figure 7